



universität
wien

MASTERARBEIT

„On the Capture of Free Floating Planets“

verfasst von

Birgit Loibnegger Bakk. rer. nat.

angestrebter akademischer Grad

Master of Science (MSc)

Wien, 2015

Studienkennzahl lt. Studienblatt:

A 066 861

Studienrichtung lt. Studienblatt:

Masterstudium Astronomie

Betreut von:

Univ.-Prof. Dr. Rudolf DVORAK

Contents

1	Abstract	3
2	Zusammenfassung	4
3	Introduction	5
4	Free-floating planets	7
4.1	Formation of a free-floating planet	9
4.2	Observations of free-floating planets	10
4.3	Free-floating planetary mass component	12
5	Numerical calculations	13
5.1	Experiment setup	14
5.1.1	Values range for the impact parameter	15
5.1.2	Initial conditions	16
5.2	Outcomes	17
5.2.1	Outcomes - graphical	19
5.2.2	Orbital elements in case of indirect flyby and indirect exchange	21
5.3	Fractal scattering	26
5.3.1	Estimating the uncertainty exponent	26
6	Statistics	29
6.1	Initial value space	30
6.1.1	Initial value space for different mass of the incoming body	30
6.1.2	Initial value space for different initial inclination of the incoming body	32
6.1.3	Initial value space for different calculation time	34
6.2	Probability of <i>flyby</i> , <i>capture</i> and <i>exchange</i>	34
6.2.1	Probability of <i>captures</i> depending on the mass of the FFP	35
6.2.2	Exponential decay of temporary captures with higher initial inclination	38
6.2.3	Exponential decay of temporary captures with time	38
7	Orbital distribution in temporary capture	40
7.1	Initial value space	40
7.1.1	Different initial inclination of the FFP	42
7.1.2	Different mass ratios	42
7.1.3	Different calculation time	44
7.2	Orbital Elements	47
7.2.1	Different mass ratio	47
7.2.2	Different initial inclination of the FFP	49
7.2.3	Different calculation time	50
7.2.4	Capture in orbits with moderate values of semi-major axis and eccentricity	51
7.2.5	Exchange of orbits	54
7.3	Prograde and retrograde orbits	55
7.3.1	Bound planet driven to retrograde orbit	57

7.4	Different initial velocity of incoming body	57
8	Summary and Conclusions	60
9	Acknowledgements	63

1 Abstract

This Master's thesis is a theoretical work about the capture of free-floating planets.

Ongoing discoveries of free-floating planetary mass objects rise the question about what can happen if such an object enters a solar-like system. Is it possible that some exoplanets are captured free-floating planets which were not born in the disk around the star they do orbit now?

In order to investigate this questions numerical computations are carried out and the interaction of a free-floating planetary mass object with a bound star-planet pair is inspected. The chosen scenario mainly happens in dense clusters where, because of the higher stellar density, the possibility that a free-floating planet enters an existing solar-like system is relatively high. (Hurley and Shara, 2002)

Therefore trajectories of a free-floating planet entering a simple bound system from infinity are calculated. The gravitational bound system consists of a sun and a Jupiter on a circular orbit. The mass of the intruding planet is varied in the range of $0.01M_{Jupiter} < M < 10M_{Jupiter}$. The initial inclination of the trajectory of the free-floating planet with respect to the orbital plane of the Jupiter is varied between 0° and 90° .

The final state of the system is determined after a certain time via calculation of the energy between the bodies in pairs and shows *capture*, *exchange* or *flyby* as possible outcomes.

It turns out that the results of the scattering process are fractal which means that slightly different initial conditions lead to different outcomes of the numerical calculations. The uncertainty exponent, α , is calculated in order to show that the process is chaotic.

In order to investigate the probabilities of *flyby*, *capture* and *exchange* a statistical analysis of the final states is made. This is carried out for different mass ratios and different initial inclinations of the incoming body. Accordingly different time scales are taken into account as well.

It is shown that a free-floating planet can be captured on prograde as well as on retrograde orbits. Furthermore cases where the capture of a free-floating planet on an orbit with moderate values of semi-major axis, eccentricity and inclination is possible are discussed. Nevertheless the capture in an orbit with high values of eccentricity or big semi-major axis is more likely.

Additionally the influence of the initial velocity of the incoming body on the probabilities of the final states is investigated. It is found, that lower velocity leads to a higher percentage of free-floating planets which end up in the state of *capture*.

2 Zusammenfassung

Diese Masterarbeit bearbeitet die Interaktion zwischen einem *free-floating planet* und einem gebundenen Stern-Planeten System. Besonders wird dabei auf den Fall eingegangen, in dem der *free-floating planet* vom System eingefangen wird und auf einer Bahn gravitativ gebunden bleibt.

Sogenannte *free-floating planets* werden laufend entdeckt. Ihre Existenz ruft einige Fragen hervor: Was kann passieren, wenn so ein Himmelskörper in ein Sonnensystem eindringt? Ist es möglich, dass einige Exoplaneten in Wirklichkeit eingefangene *free-floating planets* sind, die nicht in der Gas- und Staubscheibe um den Stern entstanden sind, um den sie jetzt kreisen?

In dieser Masterarbeit werden diese Fragen numerisch untersucht. Die Wechselwirkungen zwischen einem ungebundenen Himmelskörper mit einem gravitativ gebundenen Stern-Planeten-System werden berechnet und statistisch ausgewertet.

Das gewählte Szenario findet hauptsächlich in Galaxienhaufen statt, wo die Sterndichte höher ist und es deswegen wahrscheinlicher ist, dass ein *free-floating planet* in ein existierendes Sternsystem eindringt. (Siehe dazu: Hurley and Shara (2002))

Um das nachzustellen wird die Bahn eines gravitativ ungebundenen Planeten berechnet der in ein vereinfachtes Sternensystem eindringt. Das gravitativ gebundene System besteht aus einer Sonne und einem Jupiter, der in einer Entfernung von 1 AU auf einer kreisförmigen Bahn um den Stern kreist. Die Masse des eindringenden Planeten wird im Bereich von $0.01M_{Jupiter} < M < 10M_{Jupiter}$ variiert, ebenso wird die Neigung seiner Bahn von 0° bis zu 90° geändert um den Einfluss dieser Parameter auf den Ausgang der numerischen Berechnungen zu untersuchen.

Der Endzustand des Systems wird nach einer festgelegten Zeit mithilfe der Überprüfung der Energie des Systems festgestellt. Dabei ist der Einfang des *free-floating planets* sowie ein Vorbeiflug oder auch ein Austausch mit dem Jupiter möglich.

Es stellt sich heraus, dass die Ergebnisse fraktal sind. Das bedeutet, dass leichte Änderungen in den Anfangsbedingungen einen anderen Ausgang der numerischen Berechnung bewirken. Um die Fraktalität der Ergebnisse nachzuweisen wird der sogenannte *uncertainty exponent* berechnet.

Aufgrund der Fraktalität der Daten wird eine statistische Analyse der Ergebnisse vorgenommen und die empirische Wahrscheinlichkeit für die drei möglichen Endzustände des Systems (Einfang, Vorbeiflug, Austausch) wird berechnet. Dies wird für unterschiedliche Masseverhältnisse der beiden Planeten und unterschiedliche Bahnneigungen des eindringenden Planeten ausgeführt.

Der Einfang des zu Beginn ungebundenen Planeten ist auf prograden und retrograden Orbits möglich. Außerdem werden Fälle genauer untersucht, in denen der *free-floating planet* in einem Orbit mit niedrigen Werten der großen Halbachse und Exzentrizität eingefangen wird. Dies ist möglich, obwohl der Einfang in einem Orbit mit hohen Werten für diese beiden Bahnelemente wahrscheinlicher ist.

3 Introduction

Motivation: The universe is a huge, not to say infinite, place. It hosts lots of interest-drawing objects like pulsars, quasars, mysterious nebulae and galaxies. Those huge and bright structures and objects are more likely to draw our attention, and, to admit, are relatively easy to observe. But nevertheless, there are tiny objects floating in space, which are interesting as well. Exoplanets, colourful and each one different, which are important for our knowledge about the evolution of our own solar system. Think of our earth, a tiny little planet, at least revolving around a star, so that it is not that lonely in space as sometimes it looks like in clear nights of new moon. My Master's thesis now deals with free-floating planets. Planets, which do not orbit a star, but travel alone in the deep of our universe. Now the question arises what happens if such a free-floating object enters a bound solar-like system? Is it possible that it is captured and stays on an orbit around its new host star? Is it possible that some exoplanets are truly captured free-floating planets which did not form in the stellar disc around the star they do orbit now?

Free Floating Planets: Let's start from the beginning. One of the first reports about the evidence of such lonely drifting planetary mass objects was from Zapatero Osorio et al. (2000). They found evidence for planetary mass objects in the range of $8 - 15M_{Jupiter}$ in the relatively young ($1 - 5Myr$) σ Orionis cluster. At that time, and today as well, the boundary between brown dwarfs and planets was not really clear defined. Only for solar abundances of metallicity, the boundary between giant planets and brown dwarfs is set to $13M_{Jupiter}$ - the thermonuclear deuterium burning threshold (see section 4).

The groundbreaking statement of this report (Zapatero Osorio et al., 2000) was, that the number of free-floating planets is comparable to the number of brown dwarfs and therefore brown dwarfs and free-floating planets together could be as numerous as the stars of our Galaxy.

In the following years some other reports concerning the discovery of free-floating planetary mass objects followed:

The atmospheric features of *SOri47* observed by Zapatero Osorio et al. (1999) indicate a low surface gravity as good signs for the youth of the object which is part of the σ Orionis cluster and has a possible mass of $5 - 15M_{Jupiter}$.

Quanz et al. (2010) presented six new free-floating planetary mass candidates in the *Taurus* starforming region and for two objects determined the temperature to be $\sim 2100K$ and the mass to be in the range of $5 - 15M_{Jupiter}$.

In a wide field survey for brown dwarfs (CFBDSIR) Delorme et al. (2012b) found a late T-type dwarf potentially young because of signs of low gravity. Comparison of atmosphere models for solar metallicity yield values for the temperature in the range of $650 - 750K$ and a mass of $4 - 7M_{Jupiter}$.

Liu et al. (2013a) discovered an extremely red L dwarf in a distance of $\sim 25pc$ to the earth. For this object models give a temperature of $\sim 1160K$ and a mass of $\sim 6.5M_{Jupiter}$.

Nevertheless the formation of these objects was and is still an open question. Possible mechanisms are described in section 4.1.

But not only observational aspects of free-floating planets (concerning their mass, atmospheres, ...) yielded interesting knowledge. Also the dynamics of these free-

floating objects draws attention as scattering and ejection from their original system is one possible cause for the existence of these objects.

However, for a long time astronomers and astrophysicists have been interested in the three-body problem and further on more complex calculations of planetary systems. In the first time this was to get to know the orbits of the planets of our solar system better. For example in order to predict where Mars or Venus could be seen in the sky. So it was most important to "just" calculate orbits of planets revolving around a star and calculating trajectories of planets, which were ejected from their system. This was done in order to test the long-term stability of our solar system, for example. Calculations the other way round, where a planet enters an existing system from the outside, were not really famous. So most of the calculations concerned bound solutions and the long term stability of such orbits. Very important to mention here is the work of Poincare (1993), who dealt with the three-body problem in particular. Also interesting to mention is the work of Marchal and Bozis (1982) concerning the escape of a planet from its bound orbit.

Nevertheless, there are theories concerning the case of an incoming body, which enters an existing bound system from infinity. Important to mention here is the work of Donnison (2006) or Boyd and McMillan (1993). Mainly they focused on two special forms of the problem:

- Bound binary system and incoming body have similar masses: $m_1 \sim m_2 \sim m_3$
(Interaction of a field star with a binary-star system.)
- Bound system consisting of a massive (m_1) and a small body (m_2), incoming body is massive: $m_1 \sim m_3 \gg m_2$
(Field star (m_3) interacts with a bound planetary system.)

The third possibility of a small mass object entering an existing binary-system consisting of a massive and a small body ($m_1 \gg m_2, m_3$) has not been discussed to the same extent as the other two. This is probably because in former times planets were expected to move on bound orbits around a star. The possibility of a small body coming from infinity and interacting with a bound planetary system did not attract much of attention since the first report of a free-floating planetary mass population by Zapatero Osorio et al. (2000). Due to the difficulty to refer to free-floating low mass objects as 'planets', which obviously did not fulfil the generally accepted definition of planets, this report was regarded with scepticism in the first time. Nevertheless further on observations of such low mass objects (e.g. see Sumi et al. (2011)) and the assumptions, that such free-floating planetary mass objects are probably more common than stars (Han et al., 2004) rise the question about what will happen if such a free-floating planet enters an existing planetary system. Adams et al. (2006)) and Malmberg et al. (2007) have shown that especially in dense clusters the probability of an interaction between a free-floating planetary mass object and a bound system is non negligible.

Very interesting for me, concerning this topic, is the work of Varvoglis et al. (2012), on which my Master's thesis is based. In their article *Interaction of free-floating planets with a star-planet pair* they concentrated on the simplified coplanar case of a bound planetary system consisting of a massive star and a Jupiter-sized planet on a circular orbit and an incoming small mass object.

Only Donnison (2006), dealt with the case of an incoming planet inclined to the bound system analytically. The results found in the paper of Donnison (2006), are used in section 5.1 to determine the maximum value for the impact parameter.

In my thesis I give a brief introduction about free-floating planets. What are they? How are they created? Then a short overview about the most interesting observations of free-floating planets (section 4) is given. Afterwards the experimental setup, where the third dimension is included to the numerical calculations (section 5.1.2) is explained. In the next section (5.3) it is shown that the scattering process is fractal and the uncertainty exponent for the dataset is calculated. Then the probability of *capture* of a free-floating planet for different mass ratios as well as different initial inclination angles of the incoming body is given and calculations on longer timescales (section 6) are shown. Afterwards the orbital elements of captured free-floating planets are investigated into detail and the possible capture of such an object in a retrograde orbit (see section 7) is discussed. Accordingly a short look on what happens if the initial velocity of the incoming planet is higher or lower than the used parabolic velocity is given. In section 8 the results are discussed.

4 Free-floating planets

Free-floating planets are objects with $M < 13 M_J$ which orbits are not bound to a star. $13 M_J$ is the critical mass for thermonuclear fusion of deuterium for objects with solar metallicity. This sets the boundary between brown dwarfs ($13 M_J < 75 M_J$ - hydrogen burning threshold) and giant planets ($M < 13 M_J$). While brown dwarfs are able to fuse deuterium to ${}^3\text{He}$, giant planets do not undergo thermonuclear fusion in their interiors. Nevertheless this mass limit does not tell anything about the formation, atmospheric structure nor the interior of free-floating planets. That is why in some papers free-floating planets are called sub-brown dwarfs or planetary mass brown dwarfs. (Zapatero Osorio et al., 2001)

They are also referred to as *L-dwarfs* or *late T-type dwarfs* because without knowledge about their formation it is nearly impossible to differentiate giant planets from brown dwarfs. By optical observation it is impossible to say anything about their formation, especially, when such a low mass object orbits a star. Thus knowledge about the formation mechanisms of such low mass objects is very important to tell if such a body was formed by initial condensation of solids in a circumstellar disk (planet) or the collapse of a cloud or disk fragment. (Kroupa and Bouvier, 2003)

Free-floating planets found in the σ Orionis cluster (Zapatero Osorio et al., 2013) have temperatures between 1000 - 2300 K and dusty low gravity atmospheres of $\log(g) \sim 3.5$ which can be taken as signs of youth. Although cooler objects have been detected now; e.g. *CFBDSIR 2149-0403* with a temperature of 650-750 K and $\log(g) \sim 3.75 - 4.0$. (Delorme et al., 2012a).

In the following examples show how big the diversity of detected free-floating planetary objects is.

An interesting free-floating object was investigated by Joergens et al. (2015): *OTS 44* has a mass of $\sim 12M_{Jupiter}$, an age of $\sim 2Myr$ and is the coolest known (*M9.5*) object formed in a star-like mode. Observations of this object show significant signs of accretion and a substantial disk of $\sim 10M_{Earth}$. The process observed is similar to the one which characterizes the star-like mode of formation and was the first evidence for active accretion of a free-floating planet. Additionally this object is a unique possibility

to study disk evolution and accretion in an extreme environment.

Even more fascinating is the assumption of Badescu (2011), that it is possible, that a free-floating planet may be able to conserve a optically thick atmosphere consisting of methane, ethane and carbon dioxide, which reduces the loss of thermal energy and therefore the cooling of the planet. Thus a Jupiter-type free-floating planet may be able to keep a solvent (like water, ammonia or ethane) in a liquid state for a reasonable long time and even sustain the existence of water-based life. A numerical model for radiative energy transfer in the atmosphere for bodies smaller and larger than Earth was used and supported the assumptions. Nevertheless it has been found, that the atmosphere of such an Earth-sized body has to be two or three orders of magnitudes larger than the mass of the atmosphere of the Earth. (Badescu, 2011)

One of the first observations proving the existence of such free-floating low mass objects was by Zapatero Osorio et al. (2000). This report followed a deep optical infrared survey of the young ($1 - 5 Myr$) σ Orionis cluster (distance 352 pc from the sun), which found 18 objects with masses of $5 - 15 M_{Jupiter}$, not bound to stars. Their belonging to the cluster was confirmed with spectroscopy observations. The conclusions of the observations of Zapatero Osorio et al. (2000), that free-floating planets might be as numerous as brown dwarfs, were ground-breaking.

The first theories about the formation of free-floating planets were mostly using the theory of *ejection*. A big fraction of low mass stars is born in binary systems. If the binary has a wide separation ($> 30 AU$ - which is valid for 50% of the binary systems), the formation of planets in a protoplanetary disk around one of the binary stars is possible. For a planetary object in an orbit around one of the binary stars it is more likely to be ejected due to gravitational perturbations by the passing star (especially if the object has high eccentricity - e.g.: *16 Cygni*) than for objects around single stars. The difficulties for proving this theory are again the technical restrictions of the observation instruments, to differentiate between Jupiter-mass free-floating planets and bound Jupiters on wide orbits. Although it can be assumed, that most Jupiter-massive objects are usually observed on an orbit close to its star. (Zinnecker, 2001)

Hurley and Shara (2002) investigated this for the cluster *M22*, and concluded, that due to dynamical encounters between planetary systems and cluster stars, a large fraction of young low mass planetary objects can be ejected from their originally systems. Due to a rather low velocity dispersion, they drift outwards to the edge of the cluster on rather long time scales of $\sim 10^8$ to $\sim 10^9$ yr. This would explain the assumed high density of planetary mass objects in dense clusters. (Hurley and Shara, 2002)

To mention here is the SONYC Survey (Mužić et al., 2013) of five young star forming regions (NGC1333, ρ Ophiuchi, Chamaeleon-I, Upper Sco, and Lupus-3), where one could assume the same high density of low mass objects. In contrary to the other papers here, they observed that in NGC1333 the number of objects with $\sim 5 M_{Jupiter}$ is 20-50 times smaller than the number of stars in this region. This can be an indication for the correctness of the theory of Kroupa and Bouvier (2003), that the number of low mass objects in a cluster depends on the mechanism of formation and the circumstances of their birth.

Nevertheless, a big difficulty remains in determining the exact masses and ages of free-floating planets and how to differentiate them from brown dwarfs. This results from the difficulty in observing such faint, cool objects. With spectroscopy one can measure κ -band and Na_1 lines to determine the age of low mass objects. The correlation

between the surface gravity, the slope of the κ -band and the age is known. Also gravity sensitive alkali metal-lines can be used to determine the age of low mass objects. The only problem remaining is, that those indicators are only valid for solar metallicity (Canty et al., 2013). To determine precise masses of free-floating low mass objects, it is necessary to know the exact parallax of such an object, which is mostly impossible.

Another possibility for mass determination is, to know if an object is part of a cluster. An example for application of this method is the extremely red young *L-dwarf* *PSOJ318.5338-22.8603*, due to kinematics a member of the β Pic moving group. This object was observed with near infrared photometry and is about $12 Myr$ old. Interesting about this object is, that the unusual red colour, its luminosity and mass of $\sim 6.5 M_{Jupiter}$ coincides with the directly imaged planets *HR 8799bcd* and *2MASS J1207-39b* and tells of low surface gravity and a dusty atmosphere. (Liu et al., 2013b)

A good example for the difficulty of confirmation of a free-floating planet was described by Bennett et al. (2014) who found evidence for the first free-floating exoplanet-exomoon system. The model fitted to the microlensing event yields a ~ 4 Jupiter masses planet hosting a sub-Earth mass moon. Interesting concerning this observation is, that the data is well fitted by a model which uses a $0.12 M_{Sun}$ star with an $18 M_{Earth}$ companion, too. This example shows on the one hand, how sensitive the microlensing method is (additionally see section 4.2), but on the other hand, how difficult the determination of free-floating planetary mass objects is in fact. This is really important to mention and probably is the cause why there is a counter for exoplanets but not for free-floating planets. The confirmation of free-floating planets still is very difficult.

4.1 Formation of a free-floating planet

As already mentioned, the first theories about the formation of free-floating planets were theories about the ejection of completely developed planets from their home system. Nevertheless, this scenario is not as productive to contribute a significant number of free-floating planets observed in young clusters, because the cross-section of typical planetary systems is too small and the potential wells of the clusters are too shallow to retain the so produced free-floating planets. In the work of Kroupa and Bouvier (2003) four potential formation processes are described:

star like: collapsing cloud fragments, accretion from an envelope until feedback from the hydrostatic core halts accretion

ejection from a dynamically unstable multiple-protostellar system and the consequent loss of the accretion envelope

photoevaporation model: removal of the accretion envelope due to photoevaporation through a nearby massive star

collision: hyperbolic encounters in dense embedded clusters and thus separation of embryos from their accretion envelopes

An interesting scenario is described by Gahm et al. (2013), who made radio observations combined with near infrared of 16 so called *globulettes* in H II regions in the Rosette Nebula. These globulettes are relatively cool (line temperatures from 0.6-6K) and dense ($n_H \sim 10^4 cm^{-3}$). The masses of these globulettes were derived from extinction measurements. It turned out that the majority of globulettes has less than

$13M_{Jupiter}$. Interesting is, that all these objects show molecular line emissions. Their formation is probably a consequence of the erosion of larger structures.

Meaning that the radiation pressure of possible young massive stars can lead to a compression of the interior of the surrounding plasma and thus, to the formation of denser cloud fragments which are accelerated due to photoevaporation and driven away from the nebula. Such objects may collapse to brown dwarfs or planetary-mass objects. Because of their initially high velocities they will eventually escape their surroundings and become part of the galactic environment. However, from these observations no evidence of objects embedded in the globules was found. (Gahm et al., 2013)

Woolfson (2013), describes a different process concerning the formation of free-floating planets. The so called *capture effect*: A binary system of a star and a protostar (because it is found that most of the stars are born in binary systems or systems with more companions, (Branch, 1976)) undergoes close encounters with one another and, as a result, the protostar is ripped into small pieces, so that protoplanets can form from this small dense cloud fragments. The other theory mentioned in this paper refers to dense cluster regions, where high density regions, produced by collision of turbulent gas streams, exist. This region interacts with a new born star and forms filaments of planetary masses ($0.75M_{Jupiter}$ to $20M_{Jupiter}$), where planets can condense. These planets can now be either captured by the passing star (in orbits with initial high semi-major axis (~ 1000 AU) and high eccentricity (~ 0.9)) or can escape to become free-floating planets. (Woolfson, 2013)

4.2 Observations of free-floating planets

Observations of exoplanets, planets orbiting another star than our sun, are carried out since the 1990ies. The first potential exoplanet was found in the year 1992, a pair of rocky objects orbiting the pulsar *PSR B1257+12*. (Wolszczan and Frail, 1992) The first confirmation of an exoplanet was achieved in 1995. (Mayor and Queloz, 1995) It was a giant planet orbiting the main sequence star *51 Pegasi*.

You can do transit-observation of the lightcurves or radial-velocity measurement as well as use the timing method. Those and other techniques are described by Wright and Gaudi (2013).

However, to detect planetary objects, which do not orbit a star, is much more difficult. The detection of free-floating planets is very hard because they are very small, cool and dark objects. The best ways to detect free-floating planets so far are gravitational microlensing (Han, 2006) and direct imaging (see for example Bihain et al. (2009)). The challenge in microlensing observations of such low mass objects lies in the short duration and the rarity of lensing events (better chances of observations in direction of the galactic bulge - e.g.: Zapatero Osorio et al. (2001)). Follow up observations with photometry and spectroscopy are possible but very difficult for these faint objects (J-band magnitude of 18.2-20 e.g. for the objects mentioned by Zapatero Osorio et al. (2013)).

Photometry observations for example were carried out to find free-floating planetary objects in the Pleiades. (Zapatero Osorio et al., 2014) They used broad-band filters from 1 to $5 \mu m$ in the *J* and *H* -bands, expecting effective temperatures of these objects in the range of 900 to 2750K.

Photometric observation in the optical and near infrared was also done by Zapatero Osorio et al. (2001). One problem of using photometry for such faint red objects is

the contamination by red galaxies or red giants as well as foreground low mass L-type stars and brown dwarfs.

Spectroscopy was done as follow-up observation e.g. for the free-floating planetary candidates of the σ Orionis cluster mentioned above. (Zapatero Osorio et al., 2013) They produced optical and near infrared low resolution spectra with wavelengths coverage of 1.09–1.42 μm and in the visible 825–1000 nm.

The detection of free-floating planets is very hard as described above. Same yields true for the determination of the proper age, parallax and therefore mass of these objects which can only be determined with high uncertainty.

Possible solutions for this problems are provided by Han et al. (2004) who propose combined microlensing observations both ground based and satellite bound, which could solve the problem of the missing parallax of the observed objects. To determine the properties of an lensing object three parameters are needed: The *Einstein time scale* (equation 4.1), the *Einstein ring radius* (equation 4.2) and the projected Einstein radius on the plane of the observer (equation 4.3).

$$t_E = \frac{\theta_E}{\mu_{rel}} \quad (4.1)$$

$$\theta_E = \sqrt{\frac{4GM\pi_{rel}}{c^2 AU}} \quad (4.2)$$

$$\tilde{r} = \sqrt{\frac{4GMAU}{c^2\pi_{rel}}} \quad (4.3)$$

Where M is the mass of the lensing object. π_{rel} is the relative source-lens parallax ($\pi_{rel} = \text{AU} [D_L^{-1} - D_S^{-1}]$ where D_L and D_S are the distances to the lens and the source) and μ_{rel} the proper motion. Only t_E is measured from the light curve of the lensing event and depends on M , π_{rel} and μ_{rel} . Which means, that short duration events can also be produced by low mass stars or brown dwarfs with high proper motions.

So the measurement of θ_E and \tilde{r} are required. If these values are measured, than one can calculate the mass of the lensing object by

$$M = \frac{c^2}{4G} \tilde{r} \theta_E \quad (4.4)$$

Masses of bound earth-mass planets could be measured by a satellite launched to the L2 orbit combined with ground based observations. The proper motions can be determined by analyzing the planet-induced perturbations in lensing light curves observed from space (if the planet is bound to a host star). (Gould et al., 2003)

Han et al. (2004) show, that despite the small Einstein ring radii, observations of lensing events caused by unbound planetary masses would also be sufficient enough to determine the mass of these objects. In this case the earth-satellite baseline is big enough to measure lens parallaxes.

Concerning observations of free-floating planets are two important surveys dealing with the detection of free-floating planets via gravitational microlensing: the MOA: Microlensing Observations in Astrophysics ¹ and OGLE: Optical Gravitational Lensing Experiment survey.²

¹<http://www.phys.canterbury.ac.nz/moa/index.html>

²<http://ogle.astrouw.edu.pl/>

There are ongoing observations concerning the questions about formation of unbound planetary mass objects and the contribution of free-floating planets to the Galactic disk mass. A very promising mission is *WFIRST* (*Wild Field Infrared Survey Telescope*), which is part of the *new world-new horizons* program of NASA and is expected to launch in 2018. It is designed to perform wide-field imaging and slitless spectroscopic surveys of the near infrared. It should be sensitive enough to observe unbound planets with masses as low as Mars.³ (Sumi, 2014)

Strigari et al. (2012) estimated, that such a high cadence survey of the inner Galaxy (like *WFIRST*) could measure the number of free-floating objects greater than $1 M_{Jupiter}$ per main-sequence-star to $\sim 13\%$ and the number of objects greater than the mass of Mars to $\sim 25\%$. Also observations with *Gaia* could identify planetary mass objects with $\sim 1_{Jupiter}$. (Strigari et al., 2012)

Another promising tool for detecting free-floating planets is the *Korean Microlensing Telescope Network (KMTNet)*, which will consist of three 1.6m telescopes in South America, South Africa and Australia. With this network a 24-hour coverage of the four target fields located in the central Bulge will be possible and provide the detection of ~ 2200 microlensing events per year. Predictions say, that the *KMTNet* will detect ~ 1 Earth-mass free-floating planet per year. (Here they assume a density of one such planet per star in our Galaxy.) (Henderson et al., 2014)

4.3 Free-floating planetary mass component

It all began with the report of Zapatero Osorio et al. (2000), who presented their observations of the σ orionis cluster having an extremely red low luminosity population of young free-floating objects. They searched an area of 847 square arc minutes and measured 18 candidates of free-floating planets in this cluster with masses ranging from 5 to 15 $M_{Jupiter}$. They did photometry on this objects and found out that this objects fulfil the expectations for very young giant planets: These objects have a very low surface gravity and therefore a dusty atmosphere, all indicates the young age of this population. Based on these observations they determined a mass function for the population of free floating planets in the σ Orionis cluster. The extrapolation of this function to the galactic disk yields that isolated planets with mass range from 1 to 13 $M_{Jupiter}$ could be as numerous as brown dwarfs, so that the number of brown dwarfs and planets together can outnumber stars. However, the contribution to the total mass of the disk would be less than 10 %.

Sumi et al. (2011) presented their findings of observations of microlensing events in 10 regions towards the galactic bulge in 2011.

In this joint survey between Japan and New Zealand 50 million stars have been scanned towards the center of the Milky Way during the years 2006 and 2007, revealing evidence for up to 10 free-floating planets having roughly the mass of Jupiter. This may not seem much, but prediction models for their observation samples had only estimated 1.5 to 2.5 microlensing events for low mass lenses. Thus, in order to fit their observations they had to add a new mass population to their models. A short overview over their estimations is presented in the following.

The duration of a microlensing event is given with the following simplified equation:

³<http://wfirst.gsfc.nasa.gov/>

$$t_E \sim \sqrt{\frac{M}{M_J}} \quad (4.5)$$

And $t_E < 2 d$ for objects with masses of $M_J=9.5 \cdot 10^{-4} M_\odot$.

It is to mention here, that the duration of a microlensing event does significantly depend on the distance and transverse velocity of the lens object (see section 4.2). In the survey, they measured approximately 50 million stars in bulge fields and found 10 events which refer to low mass objects in the range of 3 to 15 Jupitermasses where no host star was found within 10 AU of the microlensing detections. With follow up observations (mainly done by direct imaging) it could be stated, that there were no host stars within 10 to 500AU.

The data was now compared to two mass functions, where they assumed models with standard galactic mass density and velocity and included the stellar, stellar remnant, brown dwarf and planetary mass population.

Therefore Sumi et al. (2011) added a new planetary mass population (derived via a δ -mass function from likelihood analysis of their data) so that the power law model now implies $1.9_{-0.8}^{+1.3}$ as many unbound or distant Jupiter mass objects as main sequence stars in the mass range $0.08 < M/M_\odot < 1$. This reveals that these planetary mass objects are at least 1.5 times as frequent as planets with host stars. (Sumi et al., 2011)

5 Numerical calculations

As shown in section 4.3, space is probably "full" of free-floating planetary objects. Since a significant number of unbound planetary mass objects in the Galactic Disk can be assumed, the probability that such a free-floating planet enters a planetary system is relatively high. The article *Interaction of free-floating planets with a star-planet pair* by Varvoglis et al. (2012), on which this work is based, deals with the different scenarios which can occur in such a case of invasion.

Varvoglis et al. (2012), did numerical calculations using a bound system consisting of two bodies: a sun-like star and a bound Jupiter-sized planet. Approaching the system from infinity is a third body of Jupiter mass. Its interactions with the planetary system are investigated. All objects were considered as pointmasses. Their calculations were limited to a 2D set, so that all three objects moved on coplanar orbits. In order to investigate the outcomes of such interactions between a free-floating planet and a bound system statistically, they performed numerous numerical experiments for different initial configurations of their system. The initial state was determined by the phase of the bound planet and the impact parameter of the incoming body. Those parameters are explained in the following section. After a certain computation time they tested the state of the system by calculating the energy between the bodies in pairs. The three possible outcomes were: *flyby*, *temporary capture* and *exchange*. The probability for each outcome was estimated for different initial configurations with different mass and different calculation time. In any case *capture* and *flyby* are most likely to occur compared to *exchange*. Important to mention is, that the scattering process is fractal, which will be shown in section 5.3.

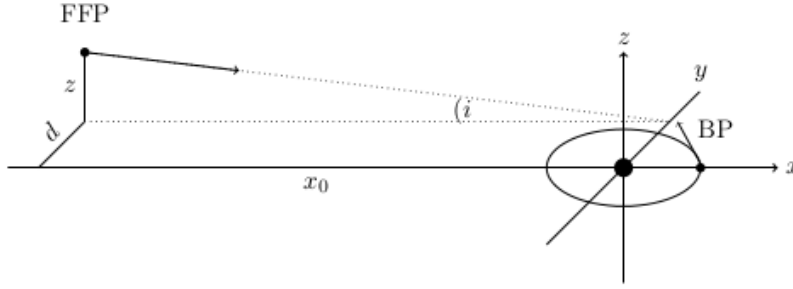


Figure 1: Initial positions of the three bodies: the sun-like star is placed at the origin, the bound Jupiter-sized planet is initially on a circular orbit with $r_0 = 1AU$ around the star and the incoming free-floating planet is started from a fixed x -distance of $x_0 = 40AU$ with a parabolic velocity. The initial state of the system is determined by the mean anomaly M of the bound planet and the y - and z -position of the free-floating planet. In this work, the y -position of the free-floating planet is referred to as *impact parameter* d of the incoming planet.

5.1 Experiment setup

Concerning the mentioned numerical calculations of the three body scattering the aim of this work is to add a third dimension to the existing setup of Varvoglis et al. (2012). Figure 1 shows the initial position of the three acting objects with respect to the inertial reference frame $0xyz$. The three bodies are considered as pointmasses. The star has mass M , on an orbit around it moves the bound planet (BP) with mass m_J and incoming from infinity is the free-floating planet (FFP) with mass m .

Star and BP are moving in the xy -plane, with the BP on an initially circular orbit with $r_0 = 1AU$. Due to the expanded setup to 3D, the FFP is coming from a position with a fixed x -distance of $40AU$, impact parameter d and initial inclination i , which is translated to a z -value corresponding to the reference frame. The initial distance of the FFP is far enough to ensure, that at the beginning of the calculations, the interaction of the FFP with the bound system is negligible, therefore one can refer to this position as *infinity*. The initial velocity, v , of the FFP is calculated as a parabolic one, via the following equation:

$$E = \frac{1}{2}mv^2 - G\frac{mM}{\sqrt{40^2 + d^2 + z^2}} = 0 \quad (5.1)$$

Keeping the other parameters fixed, the initial state of the system is determined by the impact parameter d and initial inclination i of the FFP (translated to a z -value in AU) as well as the mean anomaly M of the BP. x -, y - and z -values have the unit AU. The velocities of the objects are given in AU/d and the masses M , m and m_J are given in terms of solar masses. For better understanding, the mass of the free-floating planet is converted in Jupiter masses, when referred to it in the thesis.

The initial values of the impact parameter d are taken from the interval $-7r_0 \leq d \leq 7r_0$. This is because in this interval interactions between the FFP and the bound system are most likely to occur. It results from calculations based on the analytical analysis of the Hill stability of a three body system. Donnison (2006) provides a set of equations for finding the stability limits of a bound two body system during the encounter with a third body moving on an inclined orbit. These calculations provide

the limits on the range for the values of orbital elements for a system so that it is to remain Hill stable.

On the other hand these results tell the domain for the values of the orbital elements where close encounters between the components may happen. In my numerical integrations the values for d derived from the equations in section 5.1.1 are reused in order to get interesting results.

Hill Stability: Hill Stability is an extension of the concept of zero-velocity surfaces which were first introduced by Hill (1878) and often used for treatment of the restricted and general three-body problem (see Donnison (2006) and papers therein).

For motion in the restricted three-body problem (where one has one massless object and two massive bodies revolving around the center of mass) it is possible to derive an equation which relates the velocity of the massless particle to its position.

Zero-velocity surfaces in the restricted three-body problem correspond to a certain Jacobi constant and give the borders of the region of possible motion which cannot be crossed by an object started in this region. Donnison (2006) compares a parameter c^2E (where E is the energy of the system and c the angular momentum - which corresponds to the Jacobi constant in the restricted three-body problem) to a critical value which is found by calculation of c^2E at the position of the collinear Lagrangian points. If the value derived for c^2E is greater or equal to the critical value the system is considered as "Hill stable" which means *exchange* and *disruption* or collision of the components are not possible. (Donnison, 2006)

5.1.1 Values range for the impact parameter

As already mentioned above Donnison (2006) compares the c^2E -value of the system derived from equation 5.3 with a critical value derived from Hill surfaces, which are an extension of the zero velocity curves. Where c is the angular momentum of the system and E the total energy of the system. If the c^2E value derived is higher than the critical value, then the system is to remain stable. If the c^2E value is lower it is found that exchange or collision of the incoming bodies is possible.

The set of equations shown in the following is used to calculate the borders of the range of the orbital elements of the system, for which collision, capture or exchange can occur.

The respective system consists of three masses. M_1 and M_2 form the bound system with semi-major axis a_1 and eccentricity e_1 which in this case is set to 0, so that the BP moves on a circular orbit around its star. The third body with M_3 moves on a parabolic orbit relative to the binary barycenter with an inclination i and closest approach a_2 .

The total energy of the system, E , is calculated via the following equation:

$$E = -\frac{GM_1M_2}{2a_1} \quad (5.2)$$

The critical value for c^2E for the system is derived with the following equation:

$$S_{cr} = \frac{c^2|H|}{G^2} = \frac{f^2(x)g(x)}{2M} \quad (5.3)$$

where $M = M_1 + M_2 + M_3$ and G is the gravitational constant.

$$f(x) = M_1M_2 + \frac{M_1M_3}{1+x} + \frac{M_2M_3}{x} \quad (5.4)$$

$$g(x) = M_1M_2 + M_1M_3(1+x)^2 + M_2M_3x^2 \quad (5.5)$$

The value for x is derived as solution of the quintic equation:

$$(M_1+M_2)x^5+(3M_1+2M_2)x^4+(3M_1+M_2)x^3-(3M_3+M_2)x^2-(3M_3+2M_2)x-(M_3+M_2) = 0 \quad (5.6)$$

The parameter S_{ac} which controls the topology of the zero-velocity surfaces of the system can be written as:

$$S_{ac} = \frac{M_1M_2M_3^2\mu^2}{M} \left(\frac{a_2}{a_1} \right) + M_1^3M_2^3 \frac{(1-e_1^2)}{2\mu} + M_1^2M_2^2M_3 \cos(i) \left[\frac{2\mu(1-e_1^2)}{M} \left(\frac{a_2}{a_1} \right) \right]^{1/2} \quad (5.7)$$

The system should be Hill stable which means $S_{ac} - S_{cr} \geq 0$ which leads to the following form:

$$\frac{M_1M_2M_3^2\mu^2}{M} \left(\frac{a_2}{a_1} \right) + M_1^2M_2^2M_3 \cos(i) \left[\frac{2\mu(1-e_1^2)}{M} \right]^{1/2} \left(\frac{a_2}{a_1} \right)^{1/2} + \left[M_1^3M_2^3 \frac{(1-e_1^2)}{2\mu} - S_{cr} \right] \geq 0 \quad (5.8)$$

One can now determine the critical values of (a_2/a_1) :

$$\left(\frac{a_2}{a_1} \right) = \frac{M_1^2M_2^2M}{2M_3^2\mu^3} \left\{ \left[\left(\frac{2\mu S_{cr}}{M_1^3M_2^3} \right) - (1-e_1^2) \sin^2(i) \right]^{1/2} - (1-e_1^2)^{1/2} \cos(i) \right\}^2 \quad (5.9)$$

where $\mu = M_1 + M_2$. For $0^\circ \leq i \leq 180^\circ$ this leads to values for a_2 from $1.711r_0$ to $7.406r_0$. Which makes me choose values for the impact parameter d like the already mentioned $-7r_0$ to $7r_0$.

Impact parameters larger than this will not lead to close encounters or strong interactions between the planets. This reflects the fact, that FFPs passing at larger distances have minor effects on the planetary system. On the other hand within the calculated range *exchange* and *capture* will most likely occur.

5.1.2 Initial conditions

The initial state of the system is determined by the impact parameter d , and the initial inclination i of the FFP as well as the mean anomaly M of the BP. The initial values of the inclination for the trajectory of the FFP are varied from 0° to 90° . The impact parameter d is varied in the range of $-7r_0 \leq d \leq 7r_0$. This borders for the values of the impact parameter are derived from analytical equations, shown in section 5.1. In any case r_0 is set to be $1AU$.

The initial conditions of the three bodies are calculated as follows:

The sun is placed at rest in the center of the reference frame: $x_S = y_S = z_S = 0$ and the components of the initial velocity given as $\dot{x}_S = \dot{y}_S = \dot{z}_S = 0$.

The BP moves on a circular orbit with given initial radius of $r_0 = 1AU$ which corresponds to a period of 1 year around the star. The motion is initially started in the xy -plane. The starting point of the BP is changed by varying the mean anomaly of the BP from $0^\circ \leq \phi \leq 360^\circ$. Therefore the initial coordinates of the BP are calculated as follows:

$$x = r_0 \cos(\phi); y = r_0 \sin(\phi), z = 0$$

$$\dot{x} = -k \sin(\phi); \dot{y} = k \cos(\phi) \text{ and } \dot{z} = 0$$

With ϕ being the phase and in this case comparable to the mean anomaly of the BP and k , the Gaussian gravitational constant.

The incoming FFP has the following initial conditions:

$$x = -40r_0; y = d; z = \tan(i) \cdot x$$

$$\dot{x} = v \cos(i); \dot{y} = 0 \text{ and } \dot{z} = -v \sin(i)$$

The FFP is started on a trajectory parallel to the projected x -axis in a plane that is inclined with the value i to the xy -plane. The initial velocity v of the FFP is calculated with equation 5.1 for each initial position of the FFP.

The equations of motion are integrated with a Lie-integration method. (Hanslmeier and Dvorak, 1984)

5.2 Outcomes

Due to interactions between the incoming FFP and the bound system angular momentum between the objects (FFP and BP) can be exchanged. This can lead to three different outcomes:

Flyby: There are two types of *flyby*-motion: *indirect* and *direct* flyby. In the first case the FFP enters the system and stays in the system for some periods before being ejected back. In the case of a *direct* flyby, the incoming body passes the system without strong interactions. In both cases the FFP escapes to infinity again and the existing two body system stays bound. (For example see figure 3.)

In the following sections both cases are referred to as *flyby*. It is not distinguished between direct and indirect flyby in this work. The same yields true for *exchange*-orbits. For the analysis of the data the final state of the system after a finite time period is investigated.

Exchange: There is the possibility of an *indirect* or *direct* exchange. In the *indirect* case, the FFP is captured on an orbit around the star, forming a triple system for some periods before due to interactions between the two planets, the former BP is ejected from its system while the FFP stays on a bound orbit around the star, forming a new star-planet pair. When a *direct* exchange happens, the incoming body kicks the BP from its orbit immediately after entering the system while itself stays on a bound orbit around the star. (For example see figure 2, *left-hand* panel.)

Capture: It is the only case of bound motion, where the incoming body is captured and stays on a closed orbit around the star forming a system with two bound planets. In this case one has to be cautious, because this state may only be temporarily stable. It is better to call this final outcome *temporary capture*. Due to a close encounter between the two planets it is possible, that one gains enough energy to leave the system after some more time. In this case *temporary capture* can indirectly lead to a *flyby* or *exchange*, if calculating the system on longer time scales. (For example see figure 4 and figure 5.) *Capture* of the FFP can occur for both prograde and retrograde motion. This kind of motion will be explained and discussed in section 7.3.

Since the exit-test determines the state of the system after a certain time, if the FFP stays in *temporary capture* at this time this state of the system will be referred to as *capture*. But keep in mind, that this does only describe the state of the system at the time of the exit-test and can develop to *flyby* or *exchange* on longer time scales.

To refer all theoretically possible outcomes, the case of *disruption* has to be mentioned. In this event, the bound system breaks up and the three bodies, FFP, BP and the star would move unbound on different trajectories. This case is only possible, when the total energy of the system can switch to positive. However, this is ruled out for the following computations, because the total energy of the system at the center of mass is always negative.

The state of the system is checked after a certain time t_{test} , so that the incoming body with its initial velocity v_0 could have travelled twice its initial distance from the center of mass during this time.

$$t_{test} = \frac{2 \cdot \sqrt{40^2 + d^2 + z^2}}{v_0} \quad (5.10)$$

After this certain time, the relative energy between the three bodies in pairs is calculated, in order to determine the final state of the system as follows:

E_{ij} ... Energy between two bodies at final state for $i = 1, 2, 3$ and $j = 1, 2, 3$. Where the numbers refer to the different masses:

- 1 - free-floating planet
- 2 - star
- 3 - bound planet

- *Flyby*: $E_{12} > 0, E_{23} < 0, E_{13} > 0$
- *Capture*: $E_{12} < 0, E_{23} < 0, E_{13} > 0$
- *Exchange*: $E_{12} < 0, E_{23} > 0, E_{13} > 0$

The pairs of energies are E_{12} (FFP-star), E_{23} (star-BP) and E_{13} between FFP-BP.

Throughout the thesis, when referred to the calculation-time as t_{test} , the timespan calculated via equation 5.2 is meant. Longer time scales will be given in terms of t_{test} . Since the three possible final states of the system are only identified on the basis of the calculation of the relative energy of the objects in pairs after a finite time period it does not distinguish between *direct* or *indirect flyby* or *exchange*.

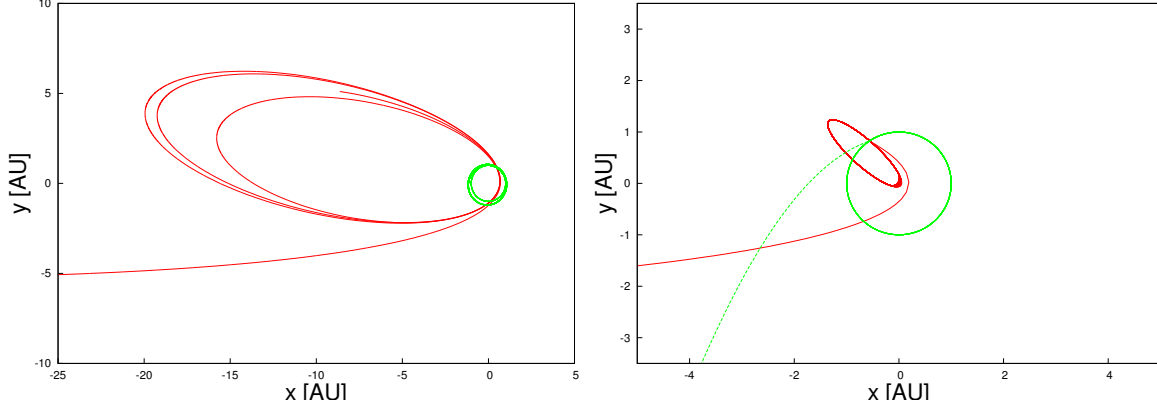


Figure 2: *Left:* Example for a *capture* - (with initial conditions: $i = 2^\circ$, mean anomaly of Jupiter $M = 90^\circ$, impact parameter $d = -5.3$, for a Jupiter-sized FFP calculated until $t = 4t_{test}$). The green line marks the orbital revolution of the BP, which is slightly perturbed from its initially circular orbit. The red line draws the trajectory of the incoming FFP, which is captured on a high eccentric orbit around the star. *Right:* Example for an *exchange* orbit - (with initial conditions: $i = 0.1^\circ$, $M = 12.1^\circ$, $d = -2.6$, $m = m_J$, calculated until $t = t_{test}$). The green line again shows the path of the BP which is ejected from the system after a close encounter with the FFP (red line), while the perturber takes its place in the bound system.

The case where the incoming body is captured as a moon of the BP ($E_{13} < 0$), did not occur in the calculations, even for masses small as $m = 10^{-8}m_J$, which is approximately the mass of our moon.

5.2.1 Outcomes - graphical

As mentioned above, there are three possible outcomes, which can occur after a certain time t_{test} . In the following figures some examples of *capture*, *exchange* and *flyby* orbits are shown, to illustrate the facts.

In figure 2 the pathways of both the FFP (red line) and the BP (green line) are plotted. In the *left-hand* panel of the figure a typical case of a *capture* event is shown. The FFP enters the bound system and stays on a highly eccentric orbit while the BP

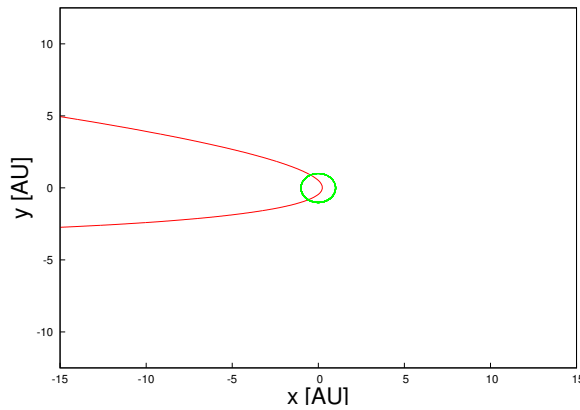


Figure 3: Example for a *direct flyby* with initial conditions of $i = 10^\circ$, $M = 150.1^\circ$, $d = -3.3$, $m = m_J$, calculated until $t = t_{test}$. The FFP passes the bound system without interacting strongly with the star-planet pair.

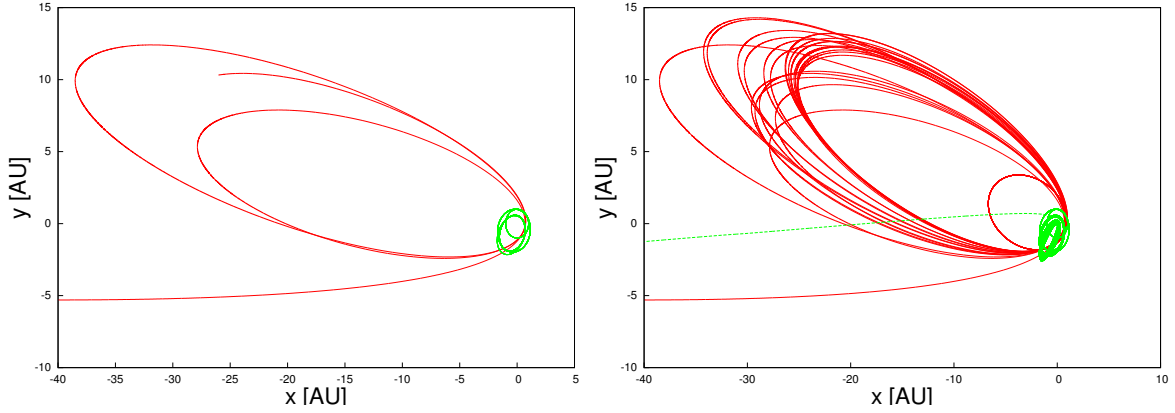


Figure 4: Example for a *capture* - (*left-hand*) - (with $i = 2.4^\circ$, $M = 90^\circ$, $d = -5.3$, $m = 5m_J$ calculated until $t = 4t_{test}$) which develops to an *exchange* - (*right-hand*) for $t = 54t_{test}$. In the *left-hand* panel the green line indicates the path of the BP, which is perturbed from its circular orbit due to the influence of the captured FFP. In the *right-hand* panel the BP is ejected from the system after some highly eccentric revolutions while the FFP's high eccentric orbit (red line) is steadied.

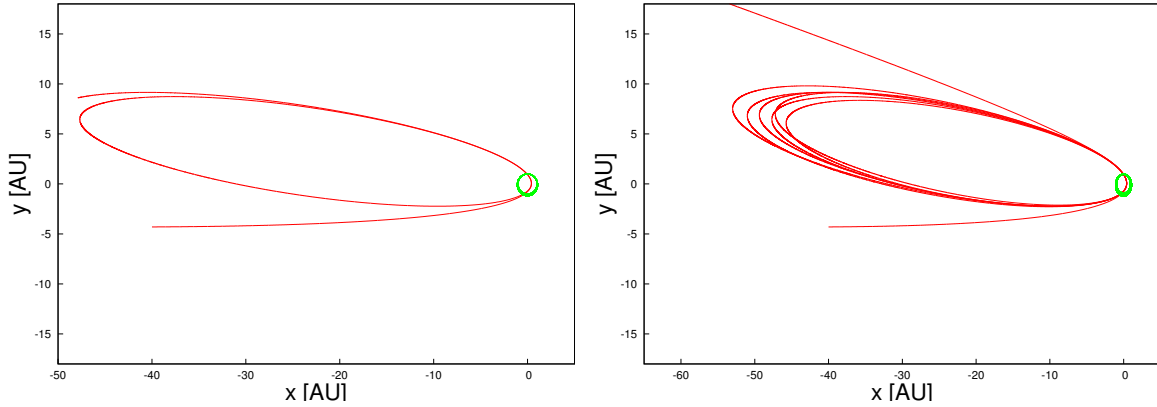


Figure 5: Example of a *capture* - (*left-hand*) - (with $i = 2.1^\circ$, $M = 204.6^\circ$, $d = -4.3$, $m = 2m_J$ calculated for $t = 6.5t_{test}$) which develops to a *flyby* - (*right-hand*) for $t = 31.5t_{test}$. The red line marks the trajectory of the FFP, which is captured on a highly eccentric orbit with big semi-major axis. After some more revolution periods it gained enough energy to leave the system again.

is slightly perturbed from its initial circular orbit. In the *right-hand* panel of the same figure an *exchange* orbit is displayed, where due to a close encounter the BP is pushed from its original orbit and forced to leave the system, while the FFP stays on a bound orbit around the star.

An example for a 'single encounter' event is shown in figure 3. In that case, the FFP interacts with the BP respectively with the bound system on a very short timescale (e.g. for a time interval less than one unperturbed revolution period of the BP). The shown case (figure 3) is a so called *direct flyby*, where the FFP passes the system of the star-BP without feeling strong attraction from it and leaving the bound system unmolested.

Nevertheless the state of the system can change, if the trajectories are calculated for even longer time scales. Examples for this can be seen in figure 4 and figure 5. Though there are 'long-time' *captures*, the possibility of a permanent capture can not be guaranteed. Figure 4 shows the path of a FFP which is captured (*left-hand* panel) on a highly eccentric orbit while disturbing the BP from its circular orbit. Calculating the same initial conditions for a longer timespan, the *temporary capture* ended in the ejection of the BP while the FFP's trajectory is relaxed to an orbit with relatively small eccentricity. This *indirect exchange* is an example for a 'multiple-encounter' event, where the FFP enters and interacts with the bound system for an extended period of time (more than one unperturbed revolution period of the BP). Figure 5 shows the second possible scenario of a 'multiple-encounter' event. The red line marks the trajectory of a FFP, captured in a highly eccentric orbit with large semi-major axis (*left-hand* panel) which, after some revolution periods leaves the system again to infinity, representing the case of an *indirect flyby*.

This illustrates the difficulty for determining a final state of the system and why the exit-test is done for most calculations after the fixed $t = t_{test}$ (see equation 5.2). The computed state of the system (pitched with the signs of the calculated relative energies) then is referred to as the final state of the system. Calculations for longer time scales were done as well in the following chapters but will be outlined clearly.

5.2.2 Orbital elements in case of indirect flyby and indirect exchange

The events of *capture* and *exchange* are mirrored in the values of the orbital elements of the acting objects. These elements in case of an *indirect flyby* is shown in figure 6 and figure 7. The plotted values show the development of the eccentricity and inclination for the trajectories of the planets in figure 5. The inclination of the FFP (see figure 6, *right-hand* panel) varies slightly around its initial value $i = 2.1^\circ$ while the inclination of the BP is pushed from $i = 0^\circ$ to a small value of $i \sim 0.1^\circ$. The same happens to the eccentricity of the BP (see figure 6, *left-hand* panel). While the FFP is captured on a highly eccentric orbit with $e > 0.9$ the BP is perturbed from its circular orbit to an orbit with eccentricity $e \sim 0.1$. In figure 7 the increasing of the eccentricity of the BP up to values higher than 0.12 via a sequence of resonances is visible. The arrow marks the point after 790 years, when due to a close encounter the FFP gains enough energy to leave the system and escape to infinity. At this point, the eccentricity of the BP drops to $e \sim 0$, but the inclination of the BP, which stays on its orbit increases slightly to $i \sim 0.2^\circ$.

The orbital elements for the event of an *indirect flyby* are plotted in figure 8 and figure 9. In figure 8 the two objects are in the condition of a *temporary capture* for the whole calculation time of $t = 4t_{test}$. Hence, since the FFP entered the system the

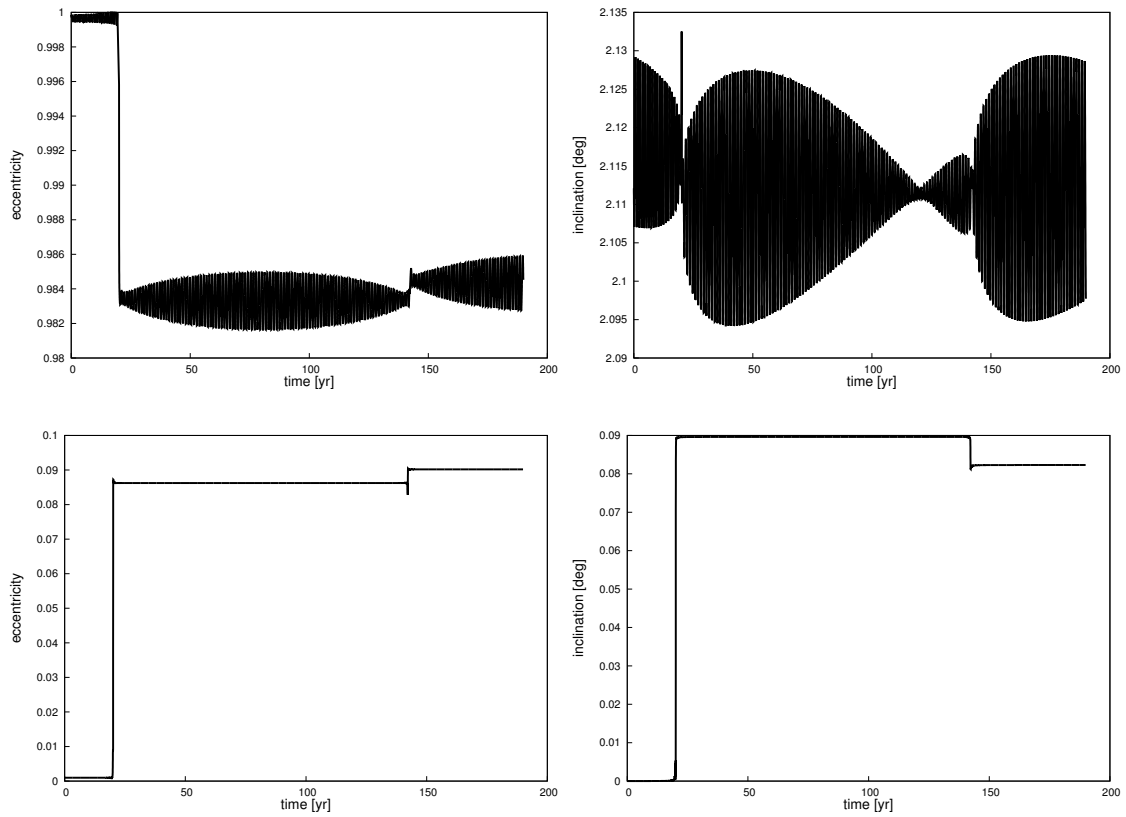


Figure 6: *Left-hand side:* Eccentricity of the FFP (*upper panel*) and the BP (*lower panel*) for the *temporary capture* orbit seen in figure 5. The system was calculated up to $t = 6.5t_{test}$ respectively ~ 190 unperturbed periods of the bound planet. The big jump of the eccentricity respectively the inclination of the BP after approximately 25 unperturbed periods (of the BP) in both panels marks the point, where the FFP enters the system.

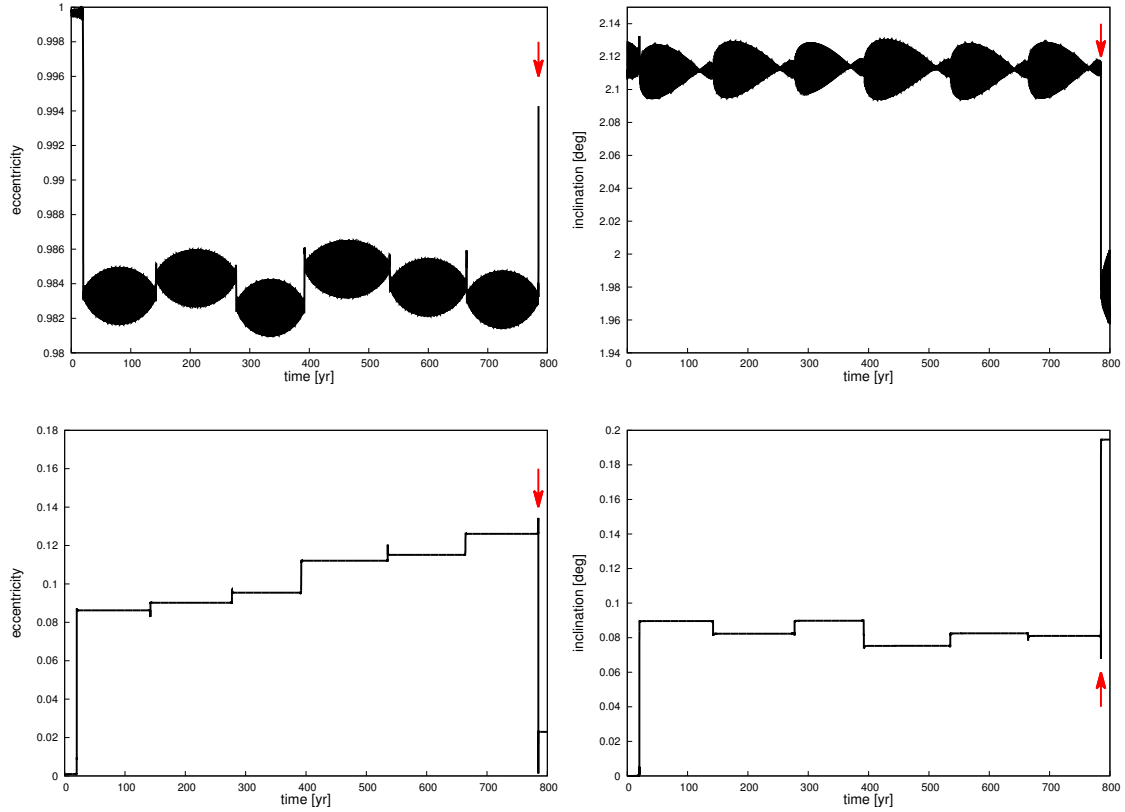


Figure 7: Evolution of eccentricity (*left-hand* panel) and inclination (*right-hand* panel) of the two involved objects for a calculation time of $t = 31.5t_{test}$. The orbital elements correspond to the case of an *indirect flyby* shown in figure 5 - *right-hand* panel. The *upper* panel shows the evolution of inclination and eccentricity of the FFP. The *lower* panel shows these orbital elements for the BP. Compared with figure 6, the eccentricity of the BP increases to values slightly higher than 0.1, before dropping to approximately zero again, at the time, the FFP is ejected from the system (arrow mark).

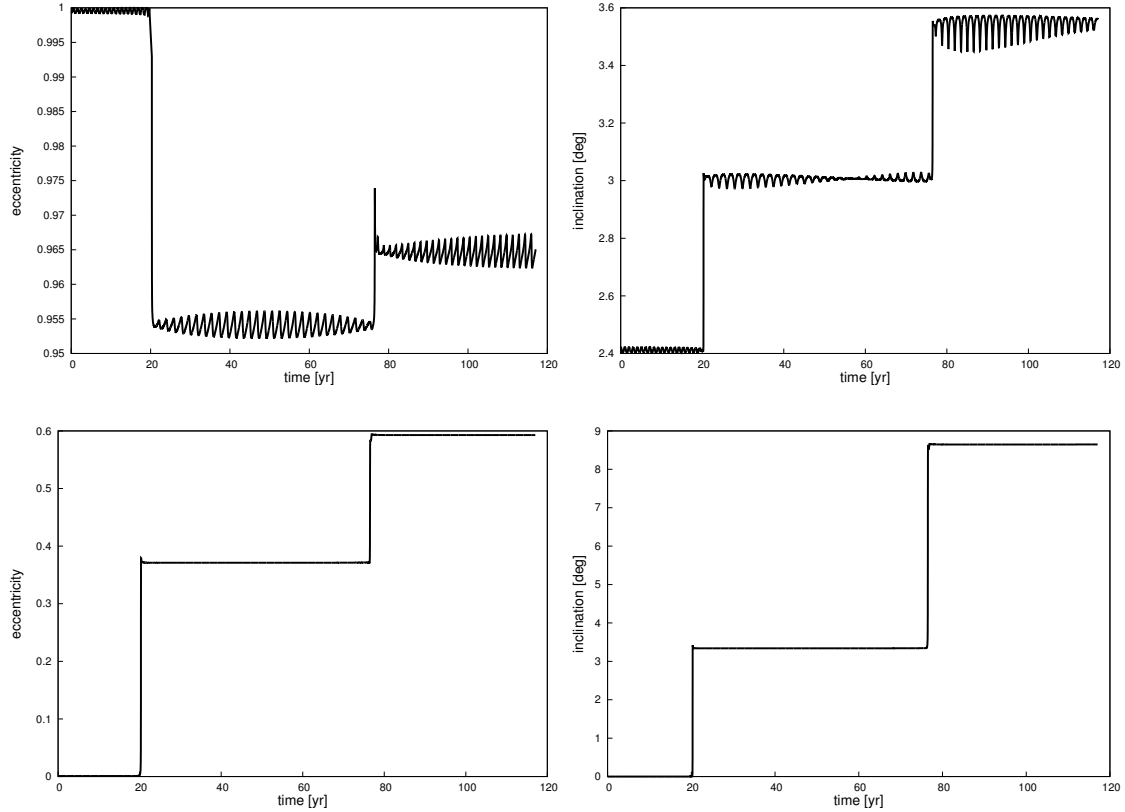


Figure 8: *Left-hand side:* Eccentricity of the FFP (*upper panel*) and the BP (*lower panel*) for the *temporary captured* orbit seen in figure 4 (left had sides), calculated up to a time of $t = 4t_{test}$. *Right-hand side:* Inclination of the two objects for the same orbit and calculation time. The first jump of the eccentricity at the time of 20 unperturbed periods of the bound planet marks the entering of the FFP into the bound system. The eccentricities of the bodies jump from one resonance to another, as do the values of the inclination. The values for the orbital elements of the BP are affected stronger, than the ones of the FFP.

planets jump from one orbital resonance to another, which is mirrored in the change of the eccentricity to higher values (for the BP up to ~ 0.68). This is a sign for the following ejection of the BP after longer calculation of the trajectories. The same behaviour can be observed in the inclination of the orbit. In the *right-hand* panel of figure 8 the line marks the evolution of the inclination of the BP reaching values as high as 8.8° while the inclination of the FFP's orbit stays close to it's initial value of 2.4° .

Calculating these trajectories for a time as long as $t = 54t_{test}$ leads to the graphs shown in figure 9. The orbit of the BP becomes more and more eccentric after a sequence of resonances until it escapes from the system (see arrow mark), while at that point the eccentricity of the captured FFP drops to $e \sim 0.78$. The increasing of the semi-major axis and the eccentricity of the BP lead to a decreasing of these orbital elements of the FFP on the other hand.

A closer look on the orbital elements of the two planets will be given in section 7 for a more statistical approach.

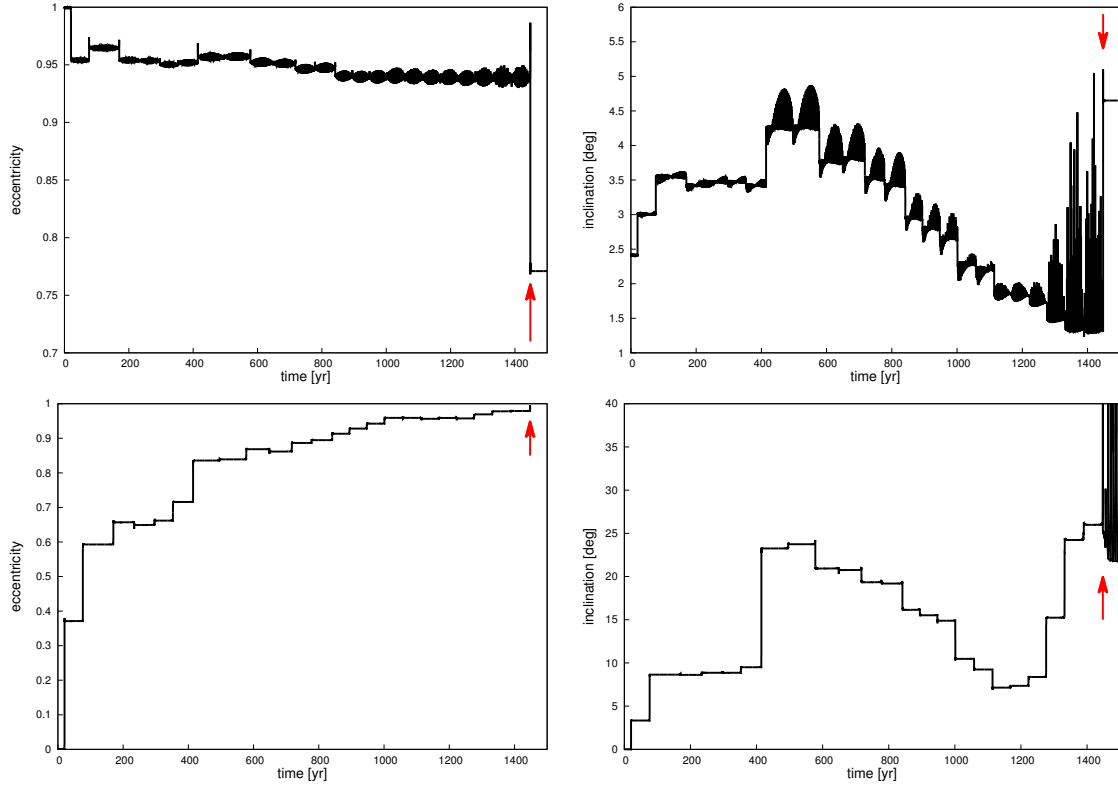


Figure 9: Development of the orbital elements of the BP and FFP in case of an *indirect exchange*. For this plot the same initial conditions as for figure 8 were calculated but to a longer time span of $t = 31.5t_{test}$. The orbit of the BP becomes more and more eccentric (see *left-hand-side, bottom panel*), jumping from one resonance to another, until it is ejected from the system (arrow mark). This event causes a relaxation of the eccentricity of the orbit of the FFP to a value of approximately 0.78 (*left-hand side, upper panel*). The same happens to the inclination of the FFP (*right-hand side, upper panel*).

5.3 Fractal scattering

In order to analyse the data statistically, calculations for the whole grid of initial conditions ($0^\circ < M < 360^\circ$ and $-7r_0 < d < 7r_0$) for a fixed initial inclination i were carried out. Therefore 3600 values of M and 1400 values of d uniformly distributed in the mentioned ranges have been chosen.

Figure 10 shows the pairs of initial conditions (M, d) for an initial inclination of the FFP of $i = 0.1^\circ$ mapped accordingly to the final state of the system after the time $2t_{test}$. Blue represents *exchange* orbits, red represents *capture* and green represents *flyby* orbits.

Figure 10 shows that *flyby* and *capture* are the most likely outcomes. *Flyby* is the final state of $\sim 42.1\%$ of systems while *capture* occurs in $\sim 56.1\%$ of all investigated cases, and is therefore (for this value of the initial inclination of the FFP) the most likely outcome. The probability of *exchange* is much smaller ($\sim 1.06\%$). These results, concerning the probability of the final states, vary with the initial inclination and mass of the FFP. Influences of these two parameters on the outcomes will be discussed in more detail in section 6.

Initial conditions leading to *exchange* are single outcomes populating the clearly defined border between the basins of the two other final states of *capture* and *flyby* (see figure 10).

In figure 11 interesting areas are enlarged. In the magnifications one can see that the boundaries do not look smooth any longer. There are scattered initial conditions in the basin of *capture* leading to a different outcome; namely *flyby* or *exchange*. This causes a great uncertainty in predicting the final state of the system for initial conditions close to the border between the basins of *flyby* and *capture*. This can be observed on smaller and smaller scales (figure 11, both panels), which is a clear sign for the fractality of the scattering process.

This sign of chaos in the results of numerical calculations concerning the interactions between a free-floating planet and an existing star-planet system was also reported by Varvoglis et al. (2012).

5.3.1 Estimating the uncertainty exponent

The fractality of the scattering process, which is shown in figures 10 and 11 can be proved by the *final state sensitivity method* (see Bleher et al. (1990)). The idea behind this is, to give the probability of making a wrong prediction of the final state of the system for initial conditions very close to each other. The separation between this initial conditions is set to be a very small value ϵ , which is called *uncertainty*. Thus, three pairs of initial conditions are checked for their final state, the two perturbed initial conditions ($\pm\epsilon$) and the unperturbed initial condition. If all three initial conditions lead to the same outcome, the conditions are called *epsilon certain*.

If only one of these three initial conditions leads to a different outcome, the set of initial conditions (the unperturbed and the two perturbed initial conditions) are called *epsilon uncertain*.

Doing this for many different sets of initial conditions close to the border and counting the number of *epsilon uncertain* cases determines the probability $f(\epsilon)$. The probability to make a wrong prediction of the final state.

If the boundary between two final states would be a smooth line, $f(\epsilon)$ would be exactly proportional to ϵ . Concerning the case of the scattering process, the edges

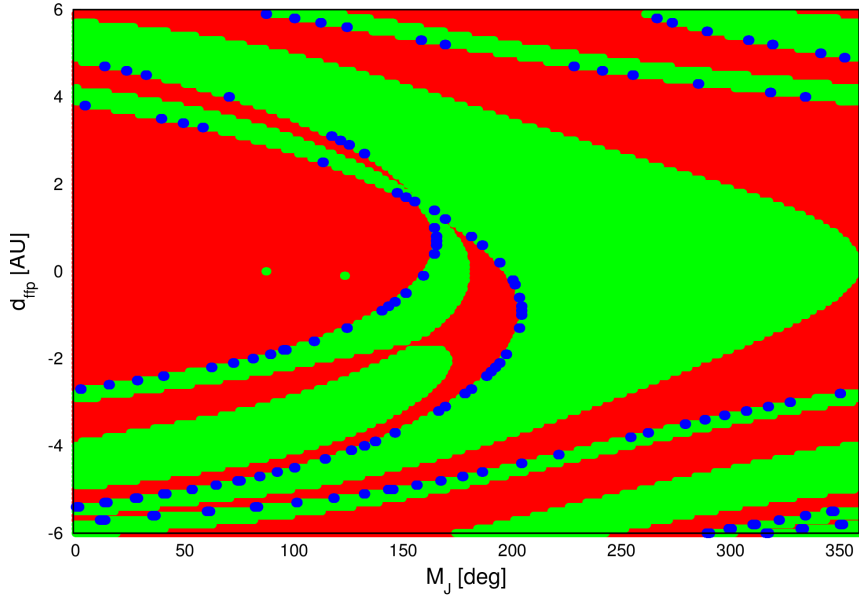


Figure 10: Initial Value Space for an experiment setup with $m = 3m_J$, $i = 0.1^\circ$. Each initial condition (M, d) is coloured, representing the final state of the system after the time $t = 2t_{test}$: Blue represents *exchange*, red *capture* and green *flyby*. The basins of initial conditions leading to *flyby* respectively *capture* are clearly separated. The borders between these basins are populated by initial conditions leading to *exchange*.

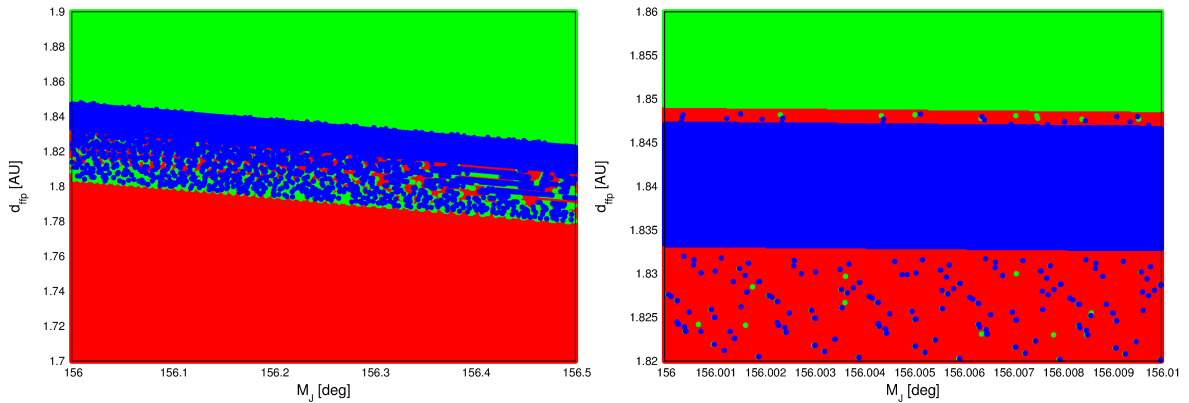


Figure 11: The *left-hand* panel shows a magnification of the initial value space shown in figure 10 for $156 < M < 156.5$ and $1.7 < d < 1.9$. The border between *flyby* and *capture* which seemed to look smooth in figure 10 shows signs of fractality which is even clearer visible in the *right-hand* panel. Here further magnification shows the initial value space for $156 < M < 156.01$ and $1.82 < d < 1.86$. Pairs of initial conditions (M, d) in the basin of *capture* (red dots) lead to different outcomes: *flyby* (green dots) or *exchange* (blue dots). This causes a great uncertainty in predicting the final state of a system for initial conditions near to the border between the basins.

between the different basins show signs of fractality and therefore the scaling of $f(\epsilon)$ with ϵ should be different. This scaling of $f(\epsilon)$ with ϵ gives the so called co-dimension of the boundary, α , with which the capacity dimension of the boundary, d , can be calculated as $d = D - \alpha$. Where D is the dimension of the embedding space.

In order to do this, 10 boxes $[\phi, d, z]$ were selected from the initial value space shown in figure 12, *left-hand* panel. In each box central initial conditions (ϕ, d, z) , the so called unperturbed initial conditions, were picked and perturbed by the amount of a small value ϵ along the y -axis. Thus the two perturbed initial conditions look like the following: $(\phi, d - \epsilon, z)$ and $(\phi, d + \epsilon, z)$.

For each of this three initial conditions (1 unperturbed, so called "central" initial condition, 2 perturbed initial conditions) the equations of motion have been calculated up to the time t_{test} and the exit-test was done in order to determine the final state of the system. After this, it is investigated if all three initial condition sets, $(\phi, d - \epsilon, z), (\phi, d, z), (\phi, d + \epsilon, z)$, lead to the same outcome. Once the systems end up in different states at the time of the exit-test, the central initial condition is considered as ϵ -uncertain.

The calculations are carried out for different values of ϵ . For each value of ϵ the fraction $f(\epsilon)$ of ϵ -uncertain central initial conditions is calculated.

The next step is to plot ϵ against $f(\epsilon)$ in a log-log diagram (see figure 12, *right-hand* panel, for box 1), where all the points $(\epsilon, f(\epsilon))$ should lie on a straight line given by the relation:

$$f(\epsilon) \sim \epsilon^\alpha \quad (5.11)$$

where α is the co-dimension of the boundary, in this case called *uncertainty exponent*. If the boundary between the basins is smooth, which means for example a straight line, α would be 1. In a case of a fractal boundary, $f(\epsilon)$ would scale different with epsilon, which is the case for the outcomes of the scattering process. Thus α should be lower than 1 and $d > 1$. With the knowledge of α , the capacity dimension d of the boundary can be calculated as follows:

$$d = D - \alpha \quad (5.12)$$

Where the dimension of the initial value space in this case is $D = 3$.

For calculation of the uncertainty dimension for the data set shown in figure 12, 10 boxes with $\delta\phi = 0.085$, $\delta d = 0.2$, $\delta i = 0.009^\circ$ are chosen from the initial value space. In each box 27.000 initial central conditions were selected and the capacity dimension of the boundary was calculated as described above for an ϵ ranging between 10^{-5} to 10^{-9} .

The function fitted to the data from figure 12, *right-hand* panel, is the following:

$$f(\epsilon) = 3.68 \cdot \epsilon^{0.51} \quad (5.13)$$

which gives the *uncertainty exponent* $\alpha = 0.51 \pm 0.056$. With this the capacity dimension d of the boundary is calculated, leading to a value of $d \simeq 2.49$, indicating a clearly fractal boundary. It can be shown, that the value for $\alpha < 1$ is derived in most cases here. This means the capacity dimension $d > 1$ and therefore the boundary is clearly fractal, as already observed in section 5.3.

The capacity dimension in the other boxes ranges between $2.12 < d < 2.56$, which fits quite well to the assumption of fractal boundaries between the different basins.

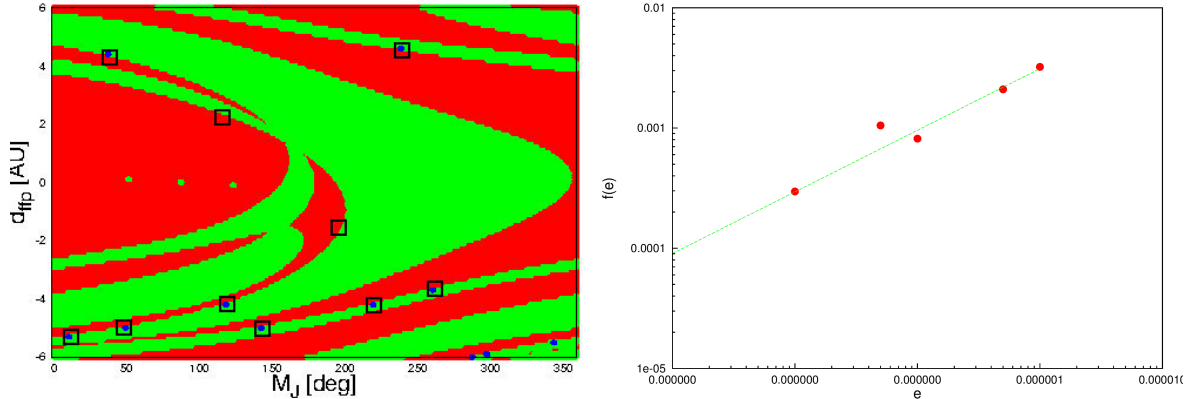


Figure 12: In the *left-hand* panel, 10 regions in which the uncertainty exponent was calculated are marked. Each box has the dimensions of $\delta\phi = 0.085$, $\delta d = 0.2$, $\delta i = 0.009^\circ$. In each box 27000 central initial conditions were chosen and perturbed by the small value ϵ . In the *right-hand* panel is a log-log diagram, plotted, of the fraction of ϵ - *uncertain* initial conditions against the used uncertainty ϵ , for region 1 (bottom left) of the grid in the *left-hand* panel. The green line indicates the fit to the data given by equation 5.13.

In order to show the fractal structure of the scattering process for the three dimensional problem the same procedure as described above was carried out for the z -value of the initial conditions. Thus from the same boxes as shown before again one central initial condition (ϕ, d, z) was taken and now the z -value was perturbed by a certain amount of ϵ , in order to get the two perturbed initial conditions $(\phi, d, z - \epsilon)$ and $(\phi, d, z + \epsilon)$. The values for the capacity dimension derived were again clearly above 1 which proofed the assumption of the fractal structure.

6 Statistics

As is shown in section (5.3), the scattering process is fractal. Thus, for a given value space of $0^\circ < M < 360^\circ$ and $-7r_0 < d < 7r_0$ the empirical probability for the three potential final states (*flyby*, *capture* and *exchange*) after a fixed integration time is determined in the following. In order to investigate the influence of mass and initial inclination of the incoming body, these parameters were varied each for a whole run over the given value space. The motivation behind this was to show how interactions between the incoming free-floating planet and the bound two-body system depend on the mass and inclination of the intruding body. The empirical probability is a good method to summarize the great amount of data derived from the computations and give a clear picture of what can be expected in case of an interaction event of a bound system with an unbound incoming planet. Additionally orbital elements in case of a *capture* (see section 7) were looked into in detail and it is shown, that retrograde orbits can occur. Furthermore the influence of the initial velocity of the incoming body on the number of *captures* is shown. Therefore, the initial velocity has been changed to higher or lower values than the parabolic velocity.

6.1 Initial value space

The initial conditions ($0^\circ < M < 360^\circ$ with $\delta M = 0.1$ and $-7r_0 < d < 7r_0$ with $\delta d = 0.1AU$) of the system are mapped to the final state (*flyby*, *capture* or *exchange*) after the scattering process in order to visualize the frequency of occurrence of the different outcomes. For different mass ratios and inclination each a full set of initial conditions is computed and the great amount of data summarized by determining the empirical probability of the three possible final states. Additionally longer integration times are tested. For better illustration of the outcomes the initial value spaces are plotted in section 6.1.1, 6.1.2 and section 6.1.3. The probabilities are explained in section 6.2. The motivation behind this was to give a graphical overview on the possible outcomes of the scattering process and show how the areas of initial conditions leading to one specific outcome shift and change with varied mass and inclination of the intruding object. Derived from this data is the empirical probability of each final state in order to quantify the graphical output.

6.1.1 Initial value space for different mass of the incoming body

In the following figures the initial value space is plotted for different mass ratios m/m_J . Each initial condition ($M, d, i = 0.1^\circ$) was calculated until t_{test} and is coloured due to the final state of the system where blue dots in the figures represent *exchange* orbits, red *capture* and green *flyby* orbits. The initial inclination of the incoming free-floating planet was fixed to $i = 0.1^\circ$ in order to reduce the amount of data. This initial inclination is converted into an initial z -distance of the FFP of $0.07AU$ from the xy -plane.

This value has been chosen per chance because it is slightly away from the plane, so that the request for three dimensional calculations is fulfilled. On the other hand it is not too far away from the xy -plane in order to not imply effects caused by higher inclinations. The influence of the initial inclination on the interaction of the FFP with the bound system is examined in section 6.1.2.

Computations were done for the initial conditions in the given range ($0^\circ < M < 360^\circ$ with $\delta M = 0.1$ and $-7r_0 < d < 7r_0$ with $\delta d = 0.1AU$) for the fixed initial inclination of the FFP. The mass of the FFP was varied in the domain of $0.0001m_J < m < 10m_J$.

In order to look for the event of the FFP being captured as a moon of the bound Jupiter, computations have been carried out for masses as low as $m = 10^{-7}m_J$, being approximately the mass of Ganymede. Nevertheless, this case has not occurred and for this reason masses lower than $0.0001m_J$ are not taken into account in the following.

The two plots in figure 13 show the initial value space for masses of the FFP of $m = 0.0001m_J$ (*left-hand side*) and $m = 0.5m_J$ (*left-hand side*). It can be seen, that the basins of initial conditions which lead to *capture* (*red*) respectively *flyby* (*green*) do not vary strongly in size and shape. For this low mass of the intruder there are no *exchange* orbits yet. Interesting is, that initial conditions leading to *flyby* are not equally distributed. This is a consequence of the varied mean anomaly, M , of the bound planet. For the same M an incoming FFP with positive impact parameter, d , encounters with different relative distance to the BP, than an incoming FFP with negative impact parameter. Therefore the exchange of angular momentum is different and this influences the final state of the system.

The initial value space for an incoming body with $m = m_J$ is plotted in the *left-hand*

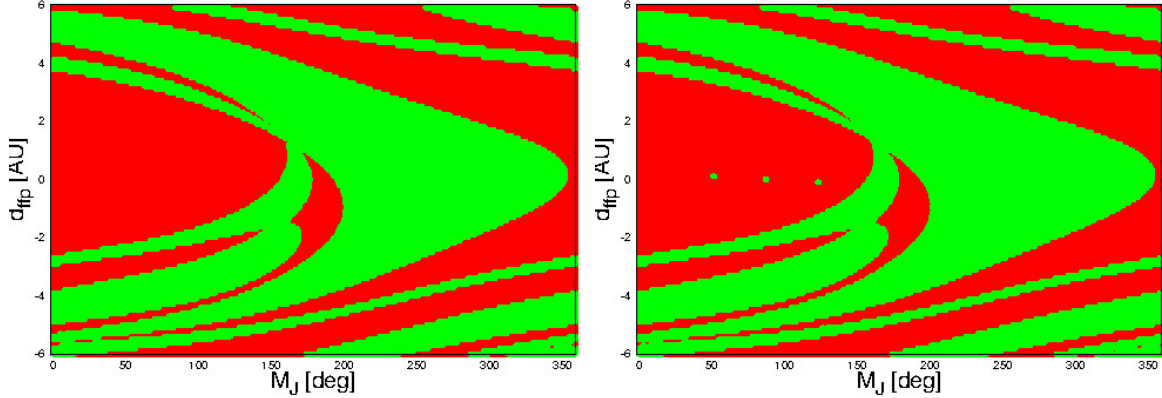


Figure 13: *Left:* Initial value space for $m = 0.0001m_J$. Red dots represent *capture*, and green *flyby* orbits. *Right:* The mass of the planet is now set to $m = 0.5m_J$. *Exchange* orbits do not occur for this low mass of the incoming planet. If one compares the *left-hand* panel with the *right-hand* panel the basins of initial conditions leading to *flyby* respectively *capture* do not change significantly.

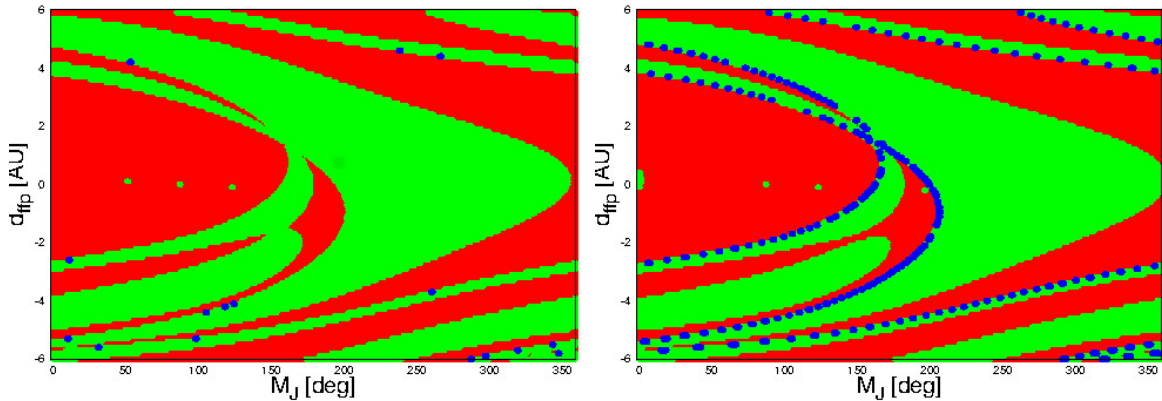


Figure 14: *Left:* Initial value space for $m = 1m_J$. Again, red dots represent *capture*, blue *exchange* and green *flyby*. The first cases of *exchange* orbits occur at the borders between the basins of *capture* and *flyby*. *Right:* Initial value space for an intruder with $m = 5m_J$.

side panel of figure 14. The first *blue* dots of initial conditions leading to an *exchange* appear for values of the impact parameter for $d < -2$ and $d > 4$.

The observation, that *exchange* orbits only occur for intruders with a mass $m > 0.5m_J$ was made by Varvoglis et al. (2012), too and is explained in detail in section 6.2.1.

For the plot in the *right-hand side* panel of figure 14 the calculations were carried out for an incoming object with $m = 5m_J$. *Exchange* orbits occur for all values of the impact parameter, d . Nevertheless most *exchange* orbits are detected for lower values of the impact parameter: $-2 < d < 2$.

Figure 15 shows the initial value space for a FFP with $m = 10m_J$. The initial conditions leading to an *exchange* are very dense at the borders between the basins leading to the other two final states. In the lower half of the plot one can see a further separation of the features in the basin of *flyby* (*green*). As the number of *exchange* orbits increases, the number of *flybys* decreases. The size of the area of initial conditions

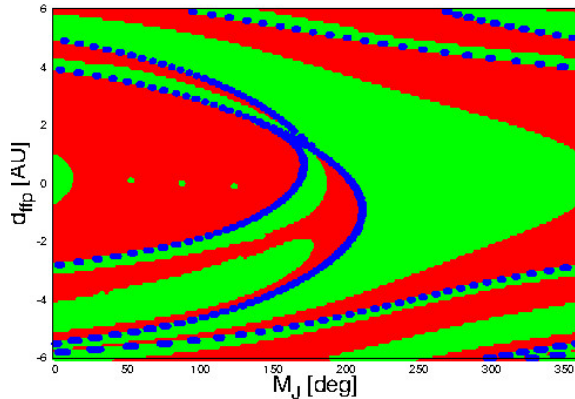


Figure 15: Initial value space for $m = 10m_J$. The number of *exchange* orbits for low values of the impact parameter d is higher than in the right panel of figure 14. For low values of $-1 < d < 1$ and the mean anomaly of the BP, $M < 20^\circ$, a basin of flyby orbits is produced and the two arms of *flyby* orbits (*green*) on the lower left side of the picture are separated.

leading to *capture* does not seem to change significantly although one could expect, that with higher mass of the FFP the probability for a *capture* would be increasing. Indeed the probability for a more massive object to be captured increases with mass. This is shown in section 6.2.1.

Concerning *exchange* orbits one could expect that the bigger the mass of the FFP, the more cases occur, where the BP is ejected from its initially bound orbit. In figure 14 and 15 the borders between the basins of *flyby* and *capture* get more and more populated by initial conditions leading to *exchange*. The bigger the mass of the incoming body, the stronger is the exchange of energy between the two planets. Thus, for a massive intruder the event of an ejection of the BP becomes more and more likely. This can be seen quantitatively in section 6.2.1.

6.1.2 Initial value space for different initial inclination of the incoming body

The influence of a possible inclination of the trajectory of the FFP, related to the orbital plane of the bound planet, on the scattering process was not investigated by Varvoglis et al. (2012), and therefore shows new results.

Motivation behind this was to generalize the knowledge about the outcomes of interactions of an unbound planet object with a bound planet-star system. As space, naturally, has three dimensions it is obvious, that a free-floating planetary object may enter an existing bound system from every possible direction. In order to investigate the influence of the inclination of the trajectory of the FFP (related to the equatorial plane of the bound system) on the outcomes of the scattering process the next set of computations was carried out changing the parameter of the initial inclination of the intruder. Therefore the angle i (see figure 1) is varied in the range of $0^\circ < i < 90^\circ$ with $\delta i = 0.1^\circ$. The mass of the FFP is fixed to $m = m_J$ and the state of the system is determined after the time t_{test} .

The influence of the initial inclination of the FFP seems to be more dramatic than the change of mass of the incoming object. The basin of *flyby* orbits (*green*) changes significantly if one compares the initial value space for an incoming planet with initial inclination of $i = 5^\circ$ (see figure 16 - *left-hand panel*) with an incoming object with

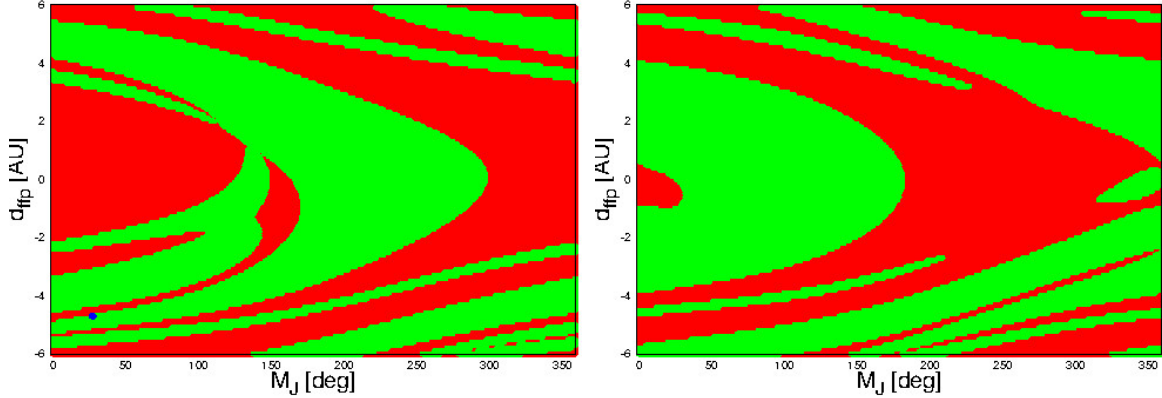


Figure 16: *Left:* Initial value space for $i = 5^\circ$. Red dots again represent *capture*, blue represents *exchange* and green represents *flyby*. The picture looks almost the same as figure 13. *Right:* The initial inclination of the FFP is set to $i = 18^\circ$. Here the basin of *capture* shrinks to systems with a initial mean anomaly of the BP of $M < 180^\circ$. The long lines of *capture* which stretch from $M = 0^\circ$ to $M = 360^\circ$ break up for higher inclinations and on the right side more separated basins for *captured* orbits occur.

$i = 18^\circ$ (figure 16 - *right-hand panel*).

The basin of *capture* grows larger and larger while the big basin of *flyby* in the left part of figure 16 - *right-hand side* - shrinks to systems with initial conditions ($M < 180^\circ$, $-4 < d < 4$). Additionally for an incoming object with $i = 18^\circ$ structures of flyby (*green*) on the right-hand side of figure 16 appear for $M > 320^\circ$. For an FFP with $i = 35^\circ$, the structures look simpler (see figure 17). The bands of initial inclination pairs seen in figure 16 leading to *flyby*, separated by small lines of initial values leading to *capture* merge for the computations made for $i = 35^\circ$ (see figure 17).

Thus for higher initial inclination of the free-floating planet the pairs of initial conditions leading to *capture* (*red dots*) look more evenly distributed. In figure 17 the basins are one big area compared to figure 16 (both panels) where the basin of *capture* is disconnected by bands of initial conditions leading to *flyby*. The structure itself, seen in figure 17 (*left hand side*) is more symmetrical except for the small gap in the area of initial conditions leading to *flyby* for $d < -4$ and $0^\circ < M < 200^\circ$.

For a initial inclination of the FFP of $i = 35^\circ$, *capture* seems to be more likely if the bound planet is started with $150^\circ < M < 280^\circ$. Compared to figure 16 (*left-hand panel*, where *flyby* is the most likely outcome in this range for the mean anomaly of the BP.)

For higher initial inclination of the FFP the biggest area for initial conditions which lead to *capture* concentrates more in the middle of the figure (see figure 17 - *right-hand side*) for low values of the impact parameter d . Thus, for FFPs with high initial inclination and high impact parameter $d > 2$ it is less likely to be captured.

Only for the initial inclination of $i = 5^\circ$ an *exchange* orbit is stated after $t = t_{test}$ (see figure 16 - *left-hand side*). For higher inclinations (figure 16 - *right-hand side* and figure 17) there are no dots which display the occurrence of *exchange* orbits.

As the exchange of angular momentum depends on the relative distance and relative velocity of the two interacting bodies one could assume that for higher inclinations of the incoming body the effect of exchange of angular momentum decreases. Thus the likelihood for an *exchange* orbit decreases as well and *flyby* becomes more probable.

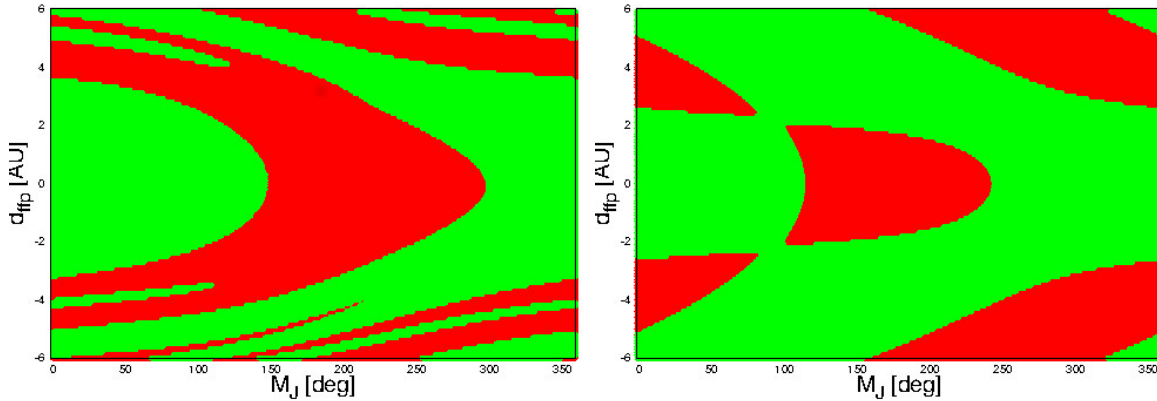


Figure 17: Initial value space for $i = 35^\circ$ on the *left-hand side*. Red represents *capture* and green *flyby*. The separated basins for *captured* systems merge on the right and on the left side of the figure. On the left side of the figure for $M < 120^\circ$ the remains of the two lines of initial conditions leading to *flyby* orbits are visible above and below the big basin of *flyby*. On the *left-hand side* the initial value space for $i = 80^\circ$ is plotted coloured according to the final state. The features look almost symmetrically. The areas for *capture* and *flyby* are big regions without any interrupting features.

6.1.3 Initial value space for different calculation time

Since it is not possible to determine if after a certain integration time the state of the system is temporary or final, the calculation time can be seen as additional parameter influencing the final state of the system. In order to investigate this influence certain sets of initial conditions have been calculated for different computation times. The initial inclination of the FFP was set to $i = 0.1^\circ$ and the mass ratio was fixed to $m/m_J = 1$. Values for the computation time were taken from the interval $[t_{test}; 17.5t_{test}]$.

In figure 18 the comparison between the shortest and the longest calculation time can be seen. The initial value space in the *left-hand side* of figure 18 shows the state of the system determined after the time t_{test} . On the *right-hand side* of figure 18 one can see the state of the system after $17.5t_{test}$.

In total the shape of the basins does not change. After the long calculation time seen on the *right-hand side* panel of figure 18, the features look more fuzzy. There are dots of initial conditions leading to *flyby* in the basin of *capture*. This characteristic is a sign for fractality of the scattering process (see section 5.3) which interestingly can be seen without magnification but for long calculation time.

6.2 Probability of *flyby*, *capture* and *exchange*

Figures 13 - 18 show, that for different values for the mass ratio m/m_J , initial inclination, i , or for the time, after which the energy-test is done in order to determine the final state of the system, the size and shape of the basins of the different outcomes vary significantly. In this section the amount of outcomes is aggregated in empirical probabilities for the three final states in order to estimate the influence of the different parameters on the final state of the system.

The figures in section 6.1 only show initial value spaces for some representative values of the investigated parameters. In order to show the effect of increased mass ratio, inclination and calculation time, empirical probabilities were calculated for values

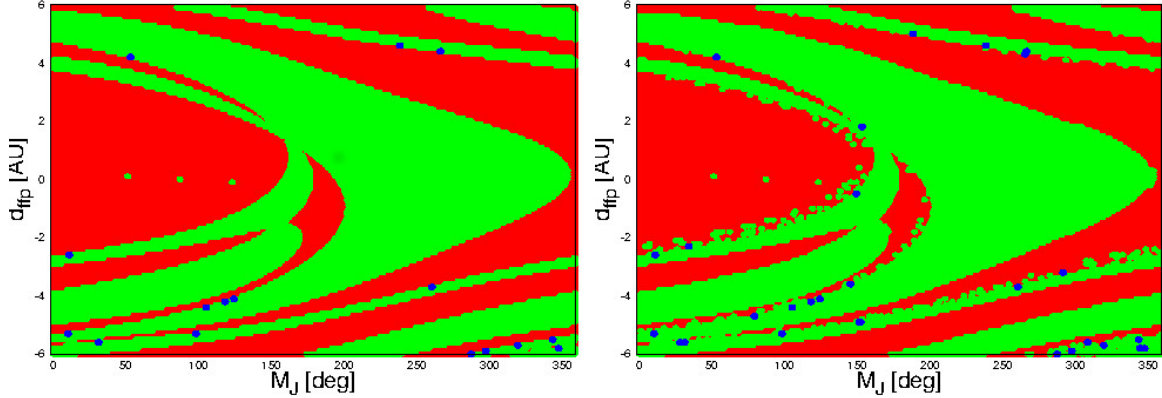


Figure 18: *Left:* Initial value space calculated until $t = t_{test}$. Red represents systems, which end up in *capture*, blue represents *exchange* and green *flyby*. For the *right-hand side panel* the trajectories were calculated for a time of $t = 17.5t_{test}$, which does not change the shape of the basins in total. The inner borders of the basins of *capture* show signs of fractality. Dots of initial conditions leading to *flyby* occur in the basin of *capture*.

all over the given ranges (see following sections).

The probabilities for *exchange*, *capture* and *flyby* in figures 19, 20 and 21 show the dependency of the likelihood for each state on the specific parameter. Each dot represents a set of 504000 different initial conditions (M, d) with M in the range of $0^\circ < M < 360^\circ$ ($\delta M = 0.1$) and $-7r_0 < d < 7r_0$ (with $\delta d = 0.1AU$).

With this given probabilities one can estimate how likely *exchange*, *capture* and *flyby* are for different incoming objects and imagine different scenarios of interaction with a free floating planet.

This may be useful for deciding if it is possible, that certain exoplanets are originally captured free-floating planets.

Important to note here again is, that the state of the system after the time t_{test} is here taken as final state, although trajectories of the bodies, which are in *temporary captured orbits* - which contribute to the percentage of *captured* free-floating planets - after this time may decay to *indirect flyby* or *indirect exchange* when calculated longer.

6.2.1 Probability of *captures* depending on the mass of the FFP

The initial inclination for these calculations is fixed to $i = 0.1^\circ$ and the determination of the final state of the system is done after t_{test} (compare section 6.1.1). The mass of the planet is chosen from values in the range of $0.0001m_J < m < 10m_J$. The chosen values are not evenly distributed as one can see. For incoming planets with a mass of $m < 2m_J$ values are chosen in smaller spacing. For planets with mass $m > 2m_J$ the increment is set to $1m_J$ with exception of the interval $[6m_J; 8m_J]$ in which the mass is increased by $\delta m = 0.5m_J$.

The *upper left-hand* panel of figure 19 shows, that for a varying ratio m/m_J approximately 55% of the initial condition sets ends up in *capture*. For higher masses ($5 M_{Jupiter}$ up to $10 M_{Jupiter}$) the probability of a *capture* is higher than for low-mass FFPs. Interesting is the minimum of the probability of being captured for objects with a mass of $3 M_{Jupiter}$.

For free-floating objects with higher masses the stronger gravitational interaction

with the bound body may be the reason for the higher percentage of bodies in captured motion. This one would expect in general: higher mass of the incoming object causing a higher probability for a *capture*. Nevertheless, the minimum of the percentage for objects with $m = 3m_J$ needs further investigation, which would have gone beyond the scope of this Master's thesis.

Approximately 1% of the calculated sets of initial conditions end up in an *exchange* orbit (see figure 19, *upper right-hand side panel*). The data shows that for incoming objects with $m < 0.5m_J$ no *exchange* orbits occur.

This fact is a result of energy conservation and can also be explained analytically, which was shown by Varvoglis et al. (2012).

Analytical explanation for lack of *exchange* orbits for incoming objects with $m < 0.5m_J$:

The incoming FFP has initially zero binding energy while the energy of the star-BP pair is given by

$$E_{23} = -\frac{GMm_J}{2r_0} \quad (6.1)$$

Thus, in case of an *exchange*, the binding energy of the new pair will be $E_{12} \leq E_{23}$ so that

$$-\frac{GMm}{2a} \leq -\frac{GMm_J}{2r_0} \quad (6.2)$$

With a being the semi-major axis of the captured FFP and r_0 the initial radius of the orbit of the BP. Solving this equation for a gives the following:

$$a \leq \frac{m}{m_J}r_0 \quad (6.3)$$

With this relation the upper boundary for values of the semi-major axis of the captured FFP can be estimated. For a mass ratio of $m/m_J = 1$ the semi-major axis of the FFP could be at most $a = 1r_0$.

These cases can be observed in section 7, which can be taken as a good sign for the accuracy of the used numerical code.

For a FFP with mass $m < 0.5m_J$ this would mean a semi-major axis of $a < 0.5r_0$. However, this value would be below the lower bound for the semi-major axis calculated with the lower bounding curve for a constant pericenter (for $a < 1$)

$$e = \frac{1}{a} - 1 \quad (6.4)$$

By setting $e = 1$ in the last equation a lower bound for the semi-major axis of $a = 0.5r_0$ is received. Thus a *direct exchange* is impossible for a FFP with $m < 0.5m_J$ (see Varvoglis et al. (2012)).

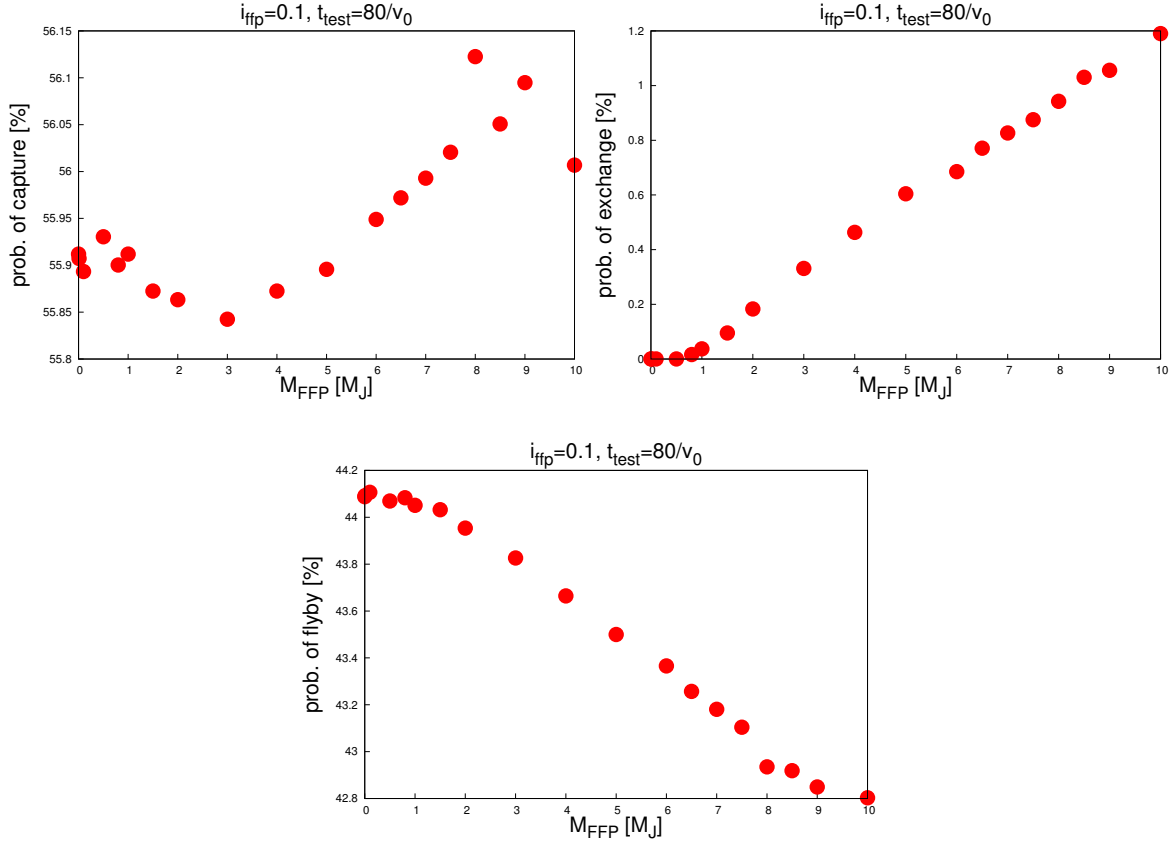


Figure 19: *Upper left-hand side:* Probability of *capture* for different mass for the incoming FFP. For masses $m < 0.5m_J$ the behaviour seems rather chaotic. From $m = m_J$ to $m = 3m_J$ the likelihood for a *capture* drops to its lowest value of 55.84%. In total the probability of *capture* varies between 55.84% and 56.12%. The minimum at $m = 3m_J$ and the high value for $m = 8m_J$ need further investigation. *upper right-hand side:* Probability of *exchange* as function of different mass of the FFP. The probability for an *exchange* - event stays lower than 1.2% while for masses of $m < 0.5m_J$ no *exchange* orbits occur. For values $m \geq 0.5m_J$ the probability of exchange seems to be a linear function of the mass. *Bottom:* Probability of *flyby* is decreasing with increasing mass ratio.

The fact, that the results from the numerical calculations reflect the analytical assumptions is a sign for the good quality of the used Lie-Integration Method. (Hanslmeier and Dvorak, 1984)

For masses $m > 0.5m_J$ the probability of *exchange* is constantly increasing. In contrary, the probability of *flyby* is decreasing with the mass of the FFP and is the supplement of the other two probabilities. (see figure 19)

However, the probabilities of *capture* and *exchange* do not vary strongly. The same is the case for the probability of *flyby*, which varies between 42.8% and 44.1% (see figure 19 - *bottom* panel). The cause for this are the small masses of the two acting planets compared to the star.

6.2.2 Exponential decay of temporary captures with higher initial inclination

The probabilities for the events of *capture*, *flyby* and *exchange* differ with the initial inclination of the incoming free-floating planet. Thus, for the calculations of the initial condition sets the value of the inclination, i , of the incoming FFP is varied in the range of $0^\circ < i < 90^\circ$. The highest inclination, for which the initial value space is calculated and analysed in order to estimate the empirical probability is $i = 88^\circ$. For $i = 90^\circ$ the free-floating planet would be started on a plane confining an angle of 90° with the xy -plane. As the FFP is started right away from the bound system this case yields no results.

For these calculations the mass of the FFP is fixed to $m = m_J$ and again the energies are calculated in pairs in order to determine the final state of the system after the time $t = t_{test}$.

For $i \leq 30^\circ$ 16 values for the initial inclination of the FFP to perform the calculations are chosen. This was in order to get more empirical probabilities for intruders with low initial inclination because of the chaotic behaviour of the scattering process, which mirrors in the probabilities (see figure 20 - both panels).

For $i > 30^\circ$ only 8 values were chosen, because for this higher values of initial inclination of the free-floating planet the trend of a decreasing probability for *capture* is clearly visible (see figure 20 - upper left-hand side).

The probabilities for the three potential outcomes are shown in figure 20. As can be seen, the probability for *capture* decreases with rising initial inclination, i , although it stays between 40% – 50% for initial inclinations with $i < 50^\circ$. For higher inclinations, $i > 50^\circ$, there seems to be a rather exponential decay of captures.

Nevertheless, the probability of a *capture* does not go to zero for values of i up to 88° . For this high initial inclination of $i = 88^\circ$ the probability of a orbit to end as *capture* is still 29.85%.

However, it is questionable if FFPs with this high initial inclination stay in the captured orbit for longer timescales since it is shown in section 7.2.4, that objects with high initial inclination occupy orbits with high values of eccentricity and semi-major axis.

On the contrary the probability for an incoming body to pass the system or escape to infinity again after some periods of revolution is increasing with initial inclination of the FFP. Thus, in general a higher initial inclination increases the probability of a *flyby*. For $i < 50^\circ$ the behaviour looks rather chaotic while there seems to be a local minimum at $i = 50^\circ$, which again would need further investigation.

Although already very low, the probability for *exchange* orbits drops to zero for an inclination higher than $i = 5^\circ$ (see figure 20 - upper right-hand side panel) and a mass ratio of the planets of $m/m_J = 1$.

6.2.3 Exponential decay of temporary captures with time

Another factor which influences the number of the three different final state orbits is the calculation time, after which the energy-test is performed. Therefore computations for longer time scales are carried out. For these investigation the initial inclination is fixed to $i = 0.1^\circ$ and the mass of the incoming FFP is set to $m = m_J$.

The *bottom* panel of figure 21 shows the empirical probability of *flyby* with time. The likelihood for an incoming object to pass the system or be ejected again after some

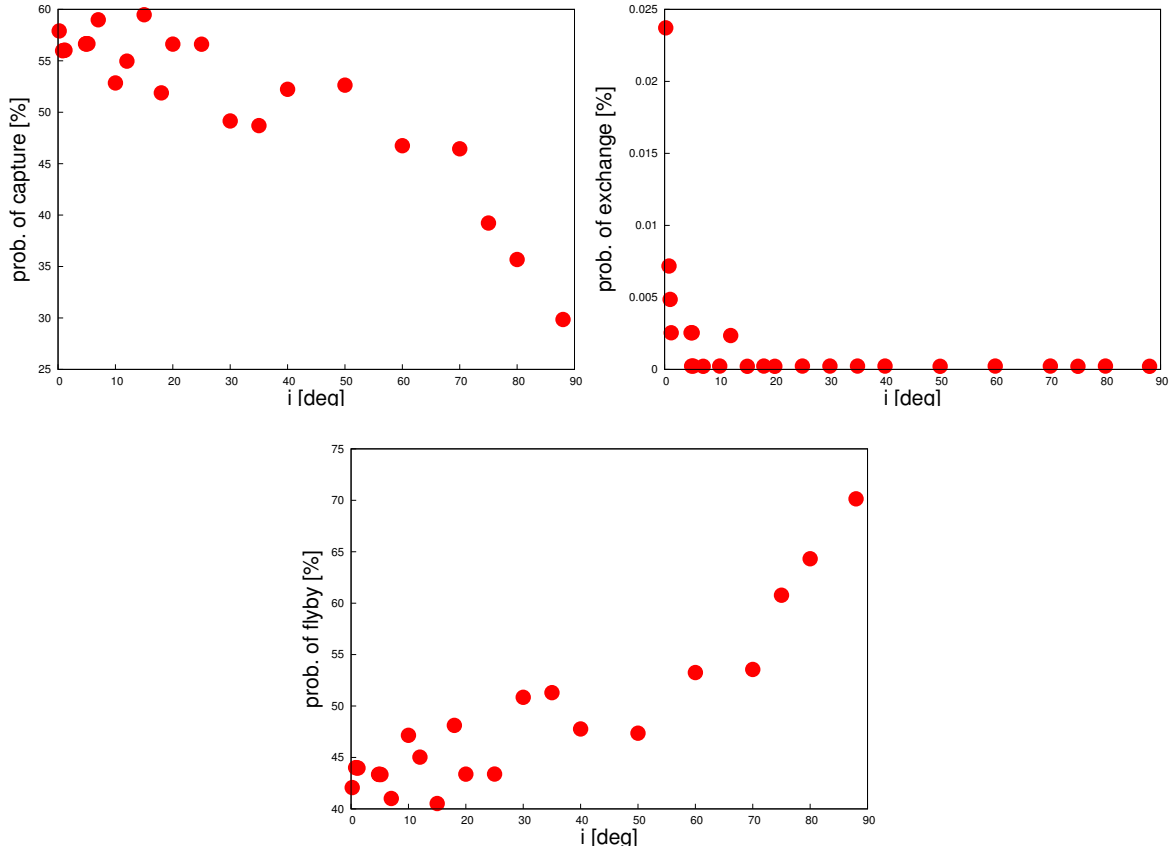


Figure 20: *Upper left-hand side:* Probability of *capture* with different initial inclination for the incoming FFP. For this computations the mass ratio is set to $m/m_J = 1$ and the final-state-test is performed after the time $t = t_{test}$. The probability of *flyby* (*bottom panel*) is an increasing function with initial inclination of the free-floating object. *Upper right-hand side:* Since the probability for an *exchange* drops from its already very low values to zero for $i > 5^\circ$ the likelihood for a *capture* is the supplement of the probability of *flyby*. Interesting is, that it does not go to zero for very high values of the initial inclination of the FFP.

revolution periods stays roughly around 42% – 44%. The *upper left-hand* panel shows the evolution of the probability of being captured which stays around 56%.

The probability of *capture* seems to be decreasing with longer integration time while the probability for *flyby* (see figure 21 - lower panel) increases by approximately 2% for integration times longer than 700 unperturbed periods of the bound planet.

The probability of *exchange* (figure 21 - *upper right hand side* panel) is the supplement of the other two with very low maximum value of 1.2%. For calculation times longer than 700 unperturbed periods of the BP the probability for an *exchange* - event drops to almost zero.

The reason for the slightly increasing probability up to the maximum value of 1.2% for an *exchange* for calculation times shorter than 700 unperturbed periods of the BP may be close encounters between the two planets (especially for planets which are captured on highly eccentric orbits) which take place after longer times. Obviously most of the FFPs captured for longer time scales than the mentioned period are ejected again from the system or stay in a captured orbit, so that no more *exchange* orbits occur.

To sum it up, integration time does not have a big influence on the final state, which can be seen in figure 21. The percentage of FFPs being in the state of *capture* at time of the energy-test which determines the final state of the system does not change strongly.

This phenomenon does not occur for higher computation times. Which shows, that the event of an *exchange* may be a result of a close encounter after a longer time span, which seems naturally, since free-floating planets with higher initial inclination are mostly captured on highly eccentric orbits with rather big semi-major axis (see section 7.2.2). Thus the planet takes longer time to come back close enough to the bound system to undergo angular momentum exchange due to a close encounter with the bound planet, which may cause the ejection of the bound Jupiter.

7 Orbital distribution in temporary capture

7.1 Initial value space

In order to show the influence of the different parameters on the final revolution direction of the FFP in a better illustrated overview the initial value spaces coloured due to the final revolution direction are shown in the the following sections. As before the grid of initial conditions is calculated for values of $0^\circ < M < 360^\circ$ with $\delta M = 0.1$ and $-7r_0 < d < 7r_0$ with $\delta d = 0.1AU$. For different mass (see section 7.1.2), different initial inclination of the intruder (see section 7.1.1) and longer integration times (see section 7.1.3) a full set of initial conditions is computed.

Motivation: As mentioned already the most common site for interaction of free-floating objects with bound systems is in dense clusters, where it is unlikely that the FFP enters the orbital plane without inclination. Thus in the following chapter the impact of the initial inclination of the intruder on its final revolution direction respectively the final revolution direction after a possible scattering with the bound planet is investigated.

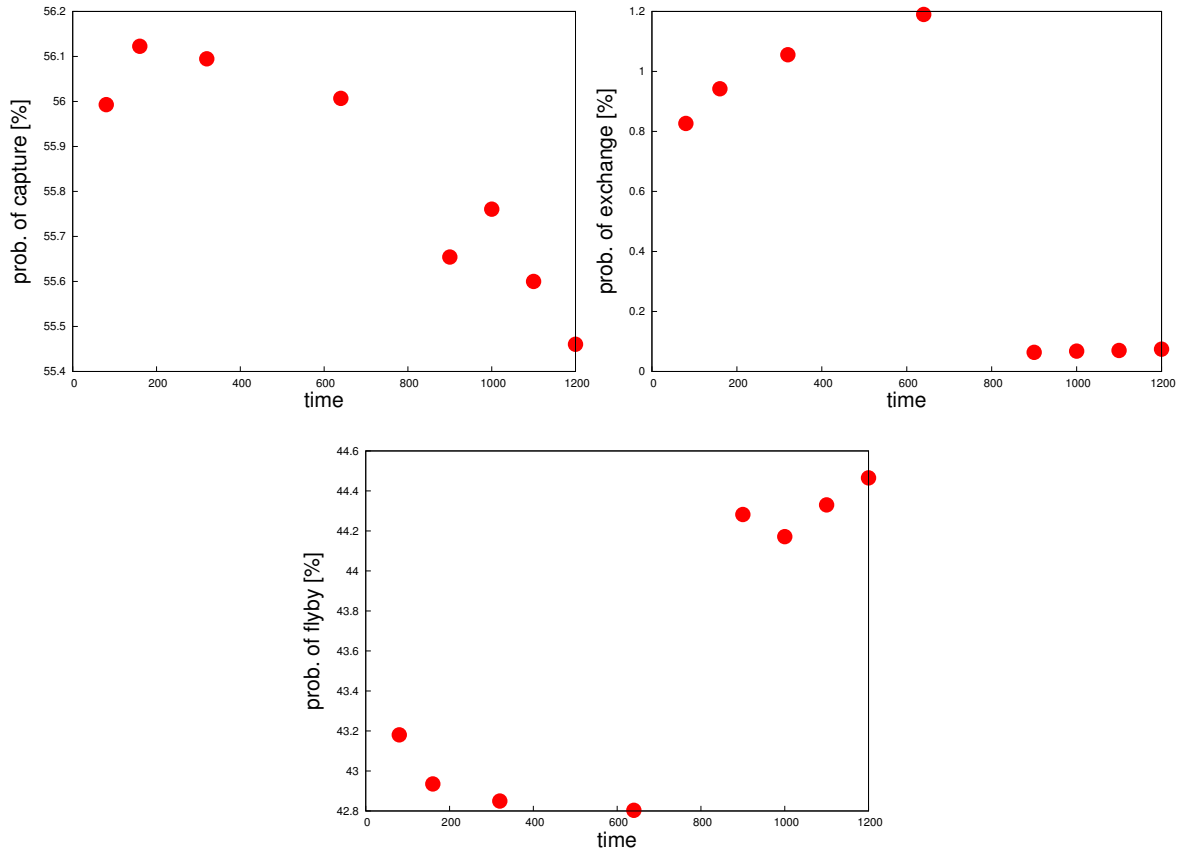


Figure 21: *Upper left:* Probability of *flyby* for longer calculation times. Time intervals on the x – *axis* here refer to one unperturbed revolution period of the BP. *Upper right:* Probability of *exchange* is a supplement to the other two, whereby the probability of an *exchange* drops to zero for calculation times longer than 700 unperturbed periods of the BP. The shown probabilities are rather constant functions with integration time. *Bottom panel:* Probability of *flyby* orbits shows only variations lower than 2%.

7.1.1 Different initial inclination of the FFP

Single values for the initial inclination were taken from the range of $0^\circ < i < 90^\circ$.

The focus in this chapter lies on the revolution direction of the FFP in case of a *capture*.

Comparing figure 30 (for a system with $i = 0.1^\circ$, $m = m_J$ after t_{test}) with figure 22 (for a system with $i = 10^\circ$, *ceteris paribus*) shows no remarkable differences in the distribution of pro- and retrograde orbits.

The small differences are as follows: Final prograde (*red*) orbits of FFPs with the given initial inclination and an impact parameter $0 < d < 0.2$ occur in the basin of retrograde (*green*) orbits for a mean anomaly of the bound planet of $M < 70^\circ$ and $M > 330^\circ$. The change of the features in general results from the higher initial inclination (see section 6.1.2).

Thus, the increase of the initial inclination does not seem to have that much influence on the final revolution direction of the FFP.

Higher inclination - examples: Qualitatively 48.12% of the captured free-floating planets with $i = 10^\circ$ end up in an orbit with prograde revolution direction compared to 47.39% of Jupiter mass objects with an initial inclination of $i = 0.1^\circ$.

The probability for the FFP of being captured in a prograde orbit shows that the picture does not change in total if increasing the initial inclination of the FFP: 48.13% of the free-floating planets with initial inclination of $i = 35^\circ$ *ceteris paribus* end up in prograde motion.

If increasing the initial inclination of the incoming object up to $i = 40^\circ$ (see figure 23), the picture looks almost the same again. In total 48.5% of the captured free-floating planets end up in prograde motion for this specific initial inclination.

Increasing the inclination up to $i = 70^\circ$ increases the probability for an orbit to end up in prograde motion to 49.89%.

Results: The exchange of angular momentum which can lead to a change in the revolution direction, depends as already mentioned on the minimum distance and the relative phase of the two bodies. Both are not that much influenced by a higher initial inclination of the FFP. Nevertheless a higher initial inclination of the incoming object makes it more likely for the FFP to be captured on a very eccentric ellipse (see section 7.2.2), which then can lead to close encounters which result in a change of the revolution direction.

7.1.2 Different mass ratios

For this section computations for free-floating planets with $m = m_J$ and $m = 10m_J$ were compared.

If the mass of the FFP is set to $m = 10m_J$ while the initial inclination is fixed to $i = 0.1^\circ$ (compare figure 30 for objects with $m = m_J$) the outcome after the time t_{test} is displayed in figure 24. Smooth spikes occur for $-0.3 < d < 0.2$ in the range of $0^\circ < M < 185^\circ$. Free-floating planets with initial parameters in the given range of (d, M) may take the opposite revolution direction of which could be expected if only looking at these initial conditions. (FFPs with an initial impact parameter $d > 0$ should end up in an retrograde orbit while FFPs with $d < 0$ should occupy a prograde orbit.)

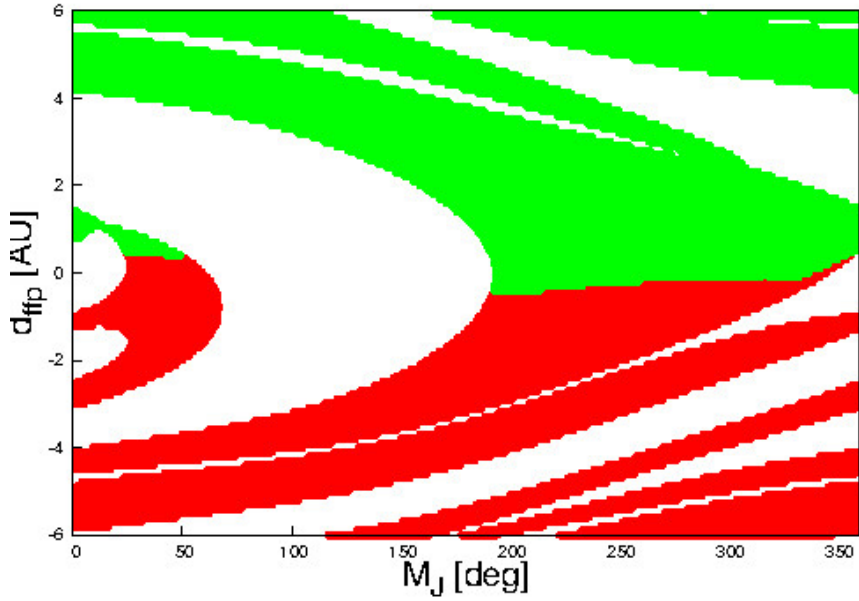


Figure 22: Proportion of *prograde* and *retrograde* orbits for $i = 10^\circ$ and $m = m_J$ after t_{test} . *Red* dots represent *prograde* and *green* represent *retrograde* orbits. The picture here looks almost the same as in figure 30 where the border between *prograde* und *retrograde* orbits is clearly defined at low values of the impact parameter of $d \sim 0$.

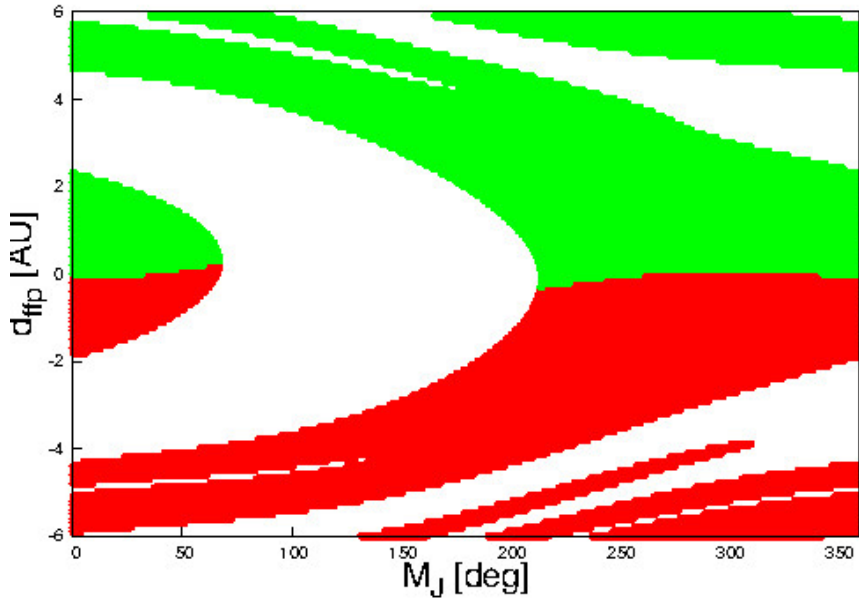


Figure 23: Proportion of *prograde* and *retrograde* orbits for $i = 40^\circ$ and $m = m_J$ after t_{test} . Again *red* dots represent *prograde* and *green* represent *retrograde* orbits. Notice, that for $260^\circ < M < 350^\circ$ there appears a small uprising, so that in this range of values FFPs with low positive impact parameter d , end up in *prograde* orbits. The same uprising can be observed in figure 22 for $260^\circ < M < 350^\circ$.

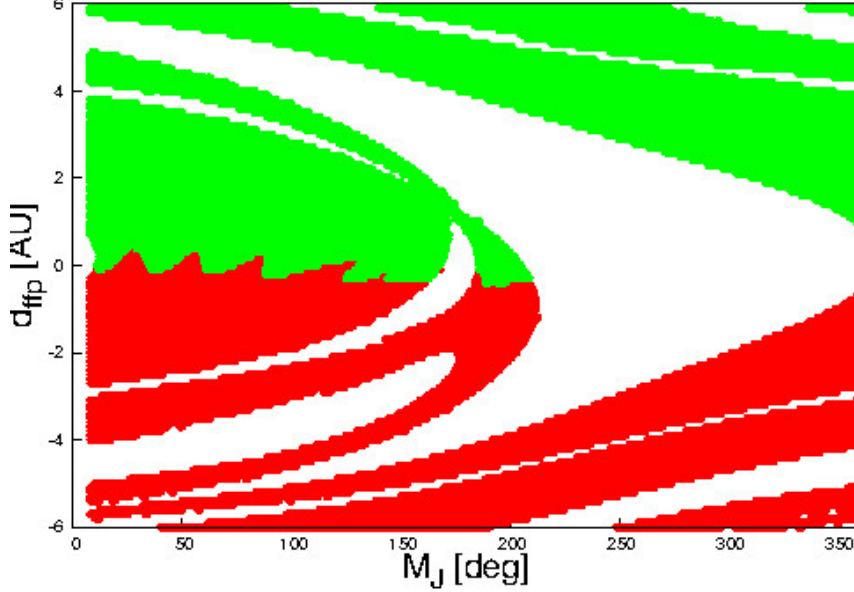


Figure 24: Proportion of *prograde* and *retrograde* orbits for $i = 0.1^\circ$ and $m = 10m_J$ after t_{test} . Red dots represent *prograde* and green dots *retrograde* orbits. Compared to the other figures prongs appear for values of $M < 150^\circ$ and $-0.2 < d < 0.5$ where initial value pairs (M, d) which should lead to *retrograde* orbits do lead to the opposite outcome.

In total 48.99% of the captured massive ($m = 10m_J$) free-floating planets end up on a prograde orbit, compared to the value of 47.39% derived before for Jupiter-sized objects.

48.55% of the FFPs end up in prograde orbits when investigating systems with initial inclination of $i = 0.1^\circ$ for the usually used computation time of t_{test} but but for a FFP five times the mass of the BP, which is a slight increase compared to computations with $m = m_J$.

Results: The more massive an intruder is, the more likely it is, that it is captured on an orbit with prograde revolution direction although it should take the opposite. Accordingly, the higher mass of the FFP shows more influence on its final orbit and the possible scattering of the BP to an orbit with opposite revolution direction.

This can be explained by taking a look on the calculated energies in pairs. For massive free-floating planetary objects the energy of the FFP-BP pair is non negligible, so the amount of energy exchanged in case of close encounters is bigger, than for low massive incoming planets.

7.1.3 Different calculation time

An interesting phenomenon occurs for longer calculation timescales (see figure 25).

Comparing the results of computations lasting for t_{test} (figure 30) to computations made for the same initial conditions ($m = m_J$ and $i = 0.1^\circ$) but calculated for $16t_{test}$ (figure 25) shows that the picture has changed completely. The occurring spikes marking trajectories of captured free-floating objects which end up on a different revolution direction than the one which could be expected concerning their initial conditions become more elongated. This can be seen in figure 25 for the whole range of mean

anomaly of the BP ($0^\circ < M < 360^\circ$) although the spikes are best visible for $M < 135^\circ$. The elongation of the spike can be seen for impact parameters d in the range of $-2.2 < d < 2.2$.

This shows that for FFPs with impact parameters $0 < d < 2.2$ (which should end up in *retrograde* motion) there are trajectories which end up on *prograde* orbits, as well as vice versa FFPs with an impact parameter $-2.2 < d < 0$ do end up in retrograde orbits.

Nevertheless statistic shows, that longer calculation time does not change the results significantly.

After $16t_{test}$ 48.83% of final orbits of the captured FFPs have prograde motion.

An explanation for this may be, that after longer computation time it is more probable, that close encounters and resulting exchange of angular momentum happen which lead to a change of revolution direction of one planet.

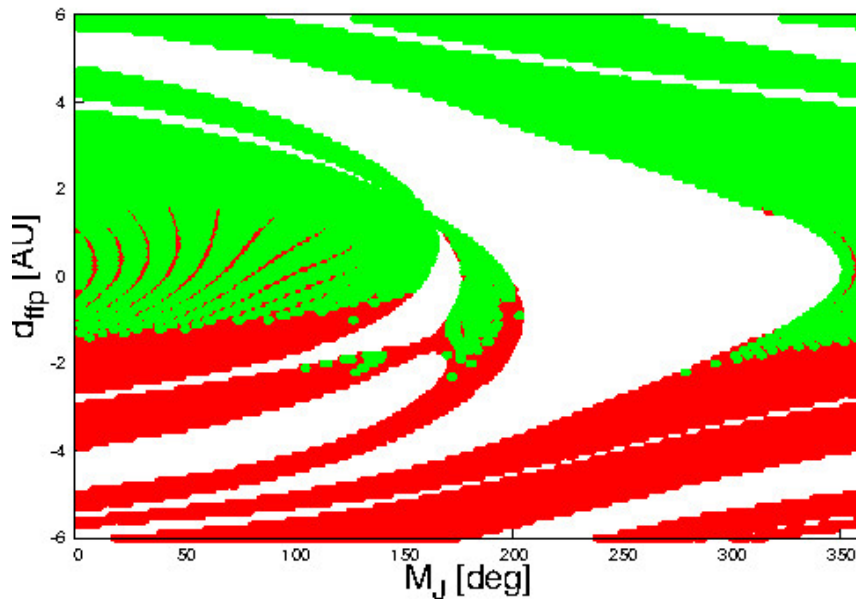


Figure 25: Proportion of *prograde* and *retrograde* orbits for $i = 0.1^\circ$ and $m = m_J$ after $t = 16t_{test}$. Red dots represent *prograde* and green dots represent *retrograde* motion. The spikes are visible for $-2.2 < d < 2.2$, where impact parameters lead to the opposite outcome of which would be expected.

Combination of mass, inclination and time: 43.38% of the FFPs end up in orbits with prograde revolution direction if computing the orbital revolution direction at time of the energy-test for a combined higher mass ($m = 5m_J$) and higher inclination ($i = 35^\circ$) of the intruder.

45.73% of the FFPs end up in prograde orbits if calculating a system with $i = 45^\circ$ and an intruder with mass of $m = 5m_J$ for as long as $t = t_{test}$.

This shows that the probability for the FFP in case of a capture to end up on a prograde orbits increases with increased inclination. Which corresponds to the trend determined in section 7.1.1.

Computing the systems for $i = 5^\circ$ and an intruder with mass of $m = 5m_J$ for as long as $t = 5t_{test}$ shows 42.99% of the FFPs ending up on a prograde orbit. Calculating

the system for $t = 50t_{test}$ ceteris paribus yields a percentage of 41.79% captured free-floating planets populating orbits with prograde revolution direction.

Example: Computations of systems with $i = 5^\circ$ and $m = m_J$ show that after t_{test} none of the bound Jupiters is driven to a revolution direction opposite to the one of its original orbit.

Calculating the systems with an intruder of $m = 10m_J$ ceteris paribus shows that 0.007% of the BP are driven to change their original revolution direction. For the same mass and after the same time but for an initial inclination of the FFP of $i = 10^\circ$ the probability drops to 0.004%.

Which shows that mass and initial inclination of the intruder have most influence on the change of revolution direction of the BP. High mass of the intruder leads to a higher percentage of bound planets which are scattered to an orbit with opposite revolution direction. Higher inclination leads to the opposite result. It can be concluded, that high mass and initial conditions which lead to close encounters support the scattering of the bound planet to an orbit with different revolution direction.

However it has to be mentioned, that those cases, where the BP takes an orbit with opposite revolution direction to its initial one may not be stable on longer time scales cause the determined values are only read out after a certain time, so that the BP may already be on its way to ejection.

Results: In general it can be said, that varying of the parameters initial inclination i , impact parameter d and mass of the incoming planet m has a slight influence on the final revolution direction. An increase of the mass and initial inclination lead to a slight increase of cases where the FFP ends up on a prograde motion, which on the other hand means a decrease of the number of retrograde orbits. Longer calculation time has the same effect. Planets with small positive and negative values of d tend to rather take the opposite revolution direction as which could be expected from their given impact parameter. This is because trajectories of these planets more often lead to close encounters and resulting exchange of angular momentum than trajectories of free-floating planets with higher impact parameters.

There exist observations of known exoplanetary systems with components moving on retrograde orbits for example Esposito et al. (2014) found the first exoplanet discovered to move on an retrograde orbit: which is *HAT-P-7b*. This fact was detected and calculated by a spin-orbit analysis which is described in Benomar et al. (2014).

As has been shown in the former section, the capture of a free-floating planet in a retrograde orbit can be reproduced by the model and integration method used for this thesis. This gives the opportunity to study scenarios of exoplanetary systems with a planet on a retrograde orbit in detail in order to find out if maybe the planet has not been formed in its present system originally but is a captured free-floating object.

In section 5.2.1 a short look on the orbital elements of the two acting planets was given for specific initial conditions in order to monitor the evolution of eccentricity, inclination and semi-major axis in case of the three potential outcomes *exchange*, *capture* and *flyby*. The following section will give a more overall view on the orbital elements at the time the integration is stopped.

7.2 Orbital Elements

The focus in this chapter lies on the case of *capture*. Thus different scenarios with different combinations of *mass ratio*, *initial inclination* and *computation time* were conducted. Again the whole grid of initial conditions (M, d) is computed for certain values of initial inclination and mass of the FFP. After a certain time the computation was stopped and the energy-test was performed. Those systems being in the state of *capture* at that time were investigated into more detail.

7.2.1 Different mass ratio

In order to investigate the influence of the mass of the incoming planetary object different masses for the free-floating planet were selected. In particular the outcomes for objects with one, five and ten Jupiter-masses were compared.

Examples: For Jupiter-sized FFPs entering the system at rather low inclinations ($i < 0.2^\circ$) the following parameters for eccentricity and semi-major axis in case of a capture were found: In most of the cases, the FFP is captured in orbits with high eccentricity ($e > 0.9$) and a semi-major axis which varies widely between $1r_0 < a < 97622r_0$. However, those rare cases with extremely large semi-major axis will most probably decay to an *indirect flyby*, after a longer integration time. Nevertheless the incoming body does not influence the orbital elements of the bound planet significantly since the results show that the BP is only slightly perturbed from its initial orbit. Nevertheless rare cases occur, in which the BP is scattered to orbits with high eccentricities and a semi-major axis up to $a_J = 818r_0$.

If one compares systems calculated for e.g. $m = m_J$, $i = 0.1^\circ$ until $t = t_{test}$ to systems calculated for $m = 10m_J$ ceteris paribus ⁴ the following can be seen:

The values for the semi-major axis measured for trajectories of the lower mass free-floating planets are determined in the range of $1.3AU < a_{FFP} < 40556AU$ with a minimum eccentricity of 0.73. The bound planet is scattered to orbits with semi-major axis of $0.99AU < a < 4.06AU$ with a maximum eccentricity of 0.89 and maximum inclination of 52.3° .

Determining the values for systems with the more massive intruder of $m = 10m_J$ yields the following: values of the semi-major axis are derived in the range of $9.95AU < a_{FFP} < 3398AU$ with minimum eccentricity of 0.92. Now the BP can be scattered to orbits with a semi-major axis in the range of $0.98AU < a < 220AU$ and a maximum eccentricity of 0.99.

Semi-major axis: In case of a *capture*, the higher the mass of the incoming planet is, the lower is the maximum semi-major axis and the larger is the minimum semi-major axis. Which means, that more massive free-floating planets populate orbits with semi-major axes in a smaller value range which is shifted away from the star.

The same yields true for the maximum semi-major axis of the final orbit of the bound planet to which it is scattered. Though the values measured do not differ more than $0.1AU$. Thus the higher the mass of the intruder is, the lower is the value which can be derived for the semi-major axis of the final orbit of the BP.

⁴Meaning: *other parameters being equal or held constant* see: https://en.wikipedia.org/wiki/Ceteris_paribus

Results suggest, that it is unlikely that hot Jupiters may be captured objects. This is based on the mentioned relation between the mass and the minimum semi-major axis. Low mass FFPs can be captured in orbits with a semi-major axis as low as $1AU$ about a star of solar mass, while the more massive ones (here up to $m = 10m_J$) only reach orbits with a semi-major axis of minimum $9.95AU$. However it is possible, that the BP is scattered to an orbit with semi-major axis of $0.98AU$ (in case of an intruder with $m = 10m_J$).

The maximum semi-major axis for a FFP with 10 times the mass of the BP is only $3378AU$ compared to the maximum semi-major axis of $40770AU$ for a FFP with a mass ratio of $m/m_J = 1$. For these orbits it is more than questionable, that this planet will stay bound on longer time scales.

Eccentricity: More massive bodies tend to be captured on orbits with higher eccentricities than intruders with lower mass. Free-floating planets with $m = m_J$ can be captured in orbits with moderate eccentricities down to 0.29. For incoming objects with $m = 10m_J$ the lowest measured eccentricity was 0.98.

Inclination: More massive intruders tend to be captured on orbits with lower values for inclination. Additionally incoming planets with higher mass (up to $m = 10m_J$) have less impact on the change of inclination of the bound planet. This may be because of the in general higher values for the semi-major axis of the orbits on which the FFP is captured and therefore the low possibility of interaction between the two planets.

It can be seen, that a more massive intruder has a bigger influence on the orbital elements of the bound planet. The more massive the incoming planet is, the bigger is the amount of energy exchanged between the two bodies in case of a close encounter.

As can be seen in figure 26, it is more likely, that an incoming FFP with a smaller mass (respectively $m = m_J$) stays on an orbit with moderate values of semi-major axis and eccentricity, than an incoming FFP with higher mass (see an incoming object with $m = 5m_J$ in figure 27 - *left-hand* panel).

This proves the common sense. One could expect, that a more massive body on its trajectory is less likely attracted by disturbing forces. The gravitational force, it feels from the smaller body is weaker, even in case of a close encounter. It takes longer to modify the trajectory of the massive FFP, which leads to high eccentric orbits.

The *left-hand* panel in figure 26 shows the orbital elements of both the BP (*green*) and the FFP (*red*) after the time t_{test} for an inclination of $i = 0.1^\circ$ and $m = m_J$. In the right hand-side panel the inclination of both of the planets at the state $t = t_{test}$ is plotted. Here it can be seen, that the BP can be perturbed from its initial coplanar orbit to an inclination as high as $i = 51.4^\circ$. Nevertheless those cases are rare and are a consequence of a close encounter. For a more massive intruder there are more cases, in which the BP is scattered to an inclined orbit, see figure 27.

For the FFP prograde as well as retrograde orbits occur (see also section 7.3) and there are orbits, in which the FFP is pushed to a higher inclination, than its initial one. Those orbits are again a consequence of close encounters and exchange of energy between the two planets.

In figure 27 orbital elements for a body with $m = 5m_J$ at the time of the energy-test ($t = t_{test}$) are plotted. Initial inclination $i = 0.1^\circ$ is the same used for the plot in figure 26. For this more massive intruder, the final orbits are shifted away from the star. The

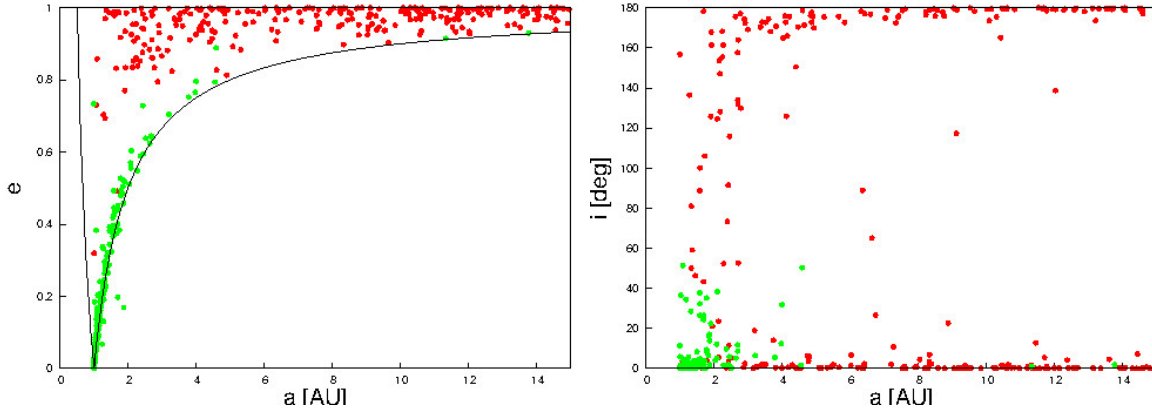


Figure 26: Distribution of orbital elements in the case of *capture* for initial conditions of $i = 0.1^\circ$, $m = m_J$ after t_{test} . *Left hand-side panel:* Semi-major axis plotted against eccentricity. *Red dots* represent the orbital elements of FFPs at the time of t_{test} . *Green dots* represent the orbital elements of the bound planet which can be disturbed from the initial circular orbit to a high extent. *Right hand-side panel:* Semi-major axis plotted against inclination. Most of the FFPs are captured in orbits with low inclination. However the BP may be disturbed from its initial plane orbit to orbits with inclinations up to $\sim 50^\circ$.

semi-major axis of the captured FFP has now values of $a > 2.4r_0$ - compare to $a > 1r_0$ for FFPs with $m = m_J$.

An incoming body with a given mass of $m = 5m_J$ can even scatter the BP to retrograde orbits with inclinations of $90^\circ < i < 134.2^\circ$, which is remarkable. The energy exchange at a close encounter can be that large, that the BP changes its revolution direction.

The solid lines in the plots concerning the orbital elements (*left-hand sides* of figure 27 and 26) represent the constant pericenter and apocenter curves, calculated with the following equations:

$$e = 1 - 1/a \text{ for } a > 1$$

$$e = 1/a - 1 \text{ for } a < 1$$

7.2.2 Different initial inclination of the FFP

As described before, the initial inclination of the FFP for the statistical approach was varied in the range of $0^\circ < i < 88^\circ$.

In general, changing the inclination of the incoming planet does not have much influence on the measured maximum semi-major axis and eccentricity of the final orbits. However, the higher the initial inclination i of the incoming FFP is, the less likely it is for the object to be captured on an orbit with moderate values of semi-major axis and eccentricity. For example for an initial inclination of the FFP of $i = 30^\circ$ (with $m = m_J$ calculated up to t_{test}) the semi-major axis for this object, if captured in an orbit around the star lies in the range of $1.93r_0 < a < 40360r_0$ with a minimum eccentricity of 0.71. The BP stays on an orbit with semi-major axis in the range of $0.99AU < a < 2.1AU$ and a maximum eccentricity of 0.56. Accordingly the BP is only scattered to orbits with an inclination of $i < 15.8^\circ$.

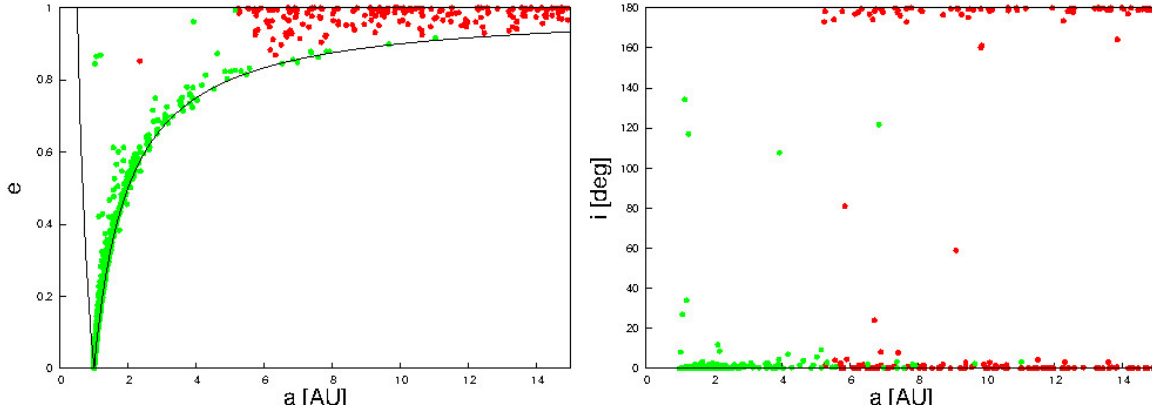


Figure 27: Distribution of orbital elements in the case of *capture* for initial conditions for $i = 0.1^\circ$, $m = 5m_J$ after t_{test} . *Left:* Semi-major axis plotted against eccentricity. Compared to figure 26 the red dots which represent the orbital elements of the FFPs after t_{test} are shifted to orbits with higher values for the semi-major axis. Less free-floating objects are captured in orbits with moderate values of eccentricity. *Right:* Semi-major axis plotted against inclination. For this setup with the more massive free-floating planets, most of the objects stay in the orbital plane with low inclination.

Compared to the example shown before the value for the minimum semi-major axis of the FFP is now higher by about $0.6AU$ while the minimum eccentricity is approximately the same. The maximum semi-major axis measured for the final orbit of the BP reduces by $\sim 2AU$ while the maximum eccentricity drops by 0.19 . The maximum inclination of the final orbit of the bound Jupiter decreases by 23.5° .

The distribution of orbital elements for a FFP with $m = m_J$ and initial inclination of $i = 30^\circ$ after $t = t_{test}$ is shown in figure 28. A rather big part of the calculated trajectories ends up in orbits with moderate values of e and a .

Compared to figure 26 this picture (figure 28) looks almost the same. This leads to the assumption a higher inclination of the incoming body does not have significant influence on the orbital elements of the planet in case of capture. Whereas the mass of the FFP has significant influence on eccentricity, semi-major axis and inclination of the final orbit (see section 7.2.1).

With increasing initial inclination of the incoming body up to $i = 80^\circ$, the semi-major axis has values in the range of $1000AU < a < 92543AU$ with additional minimum eccentricity of 0.99 . It is questionable if objects revolving around the star on an orbit with this values for semi-major axis and eccentricity will not leave the system again after some time.

On the other hand the BP stays on its circular orbit at $1AU$. This shows, that the two planets do not really interact with each other and the probability for free floating planets with initial high inclination to stay captured on longterm stable orbits is most unlikely.

7.2.3 Different calculation time

Different calculation time was applied to the initial value space for an incoming object with $m = m_J$ and an initial inclination $i = 0.1^\circ$. As described above (section 6.1.1) this value for the initial inclination was taken per chance in order to fulfil the requirement for three dimensional computations but imply no effects caused by higher inclinations.

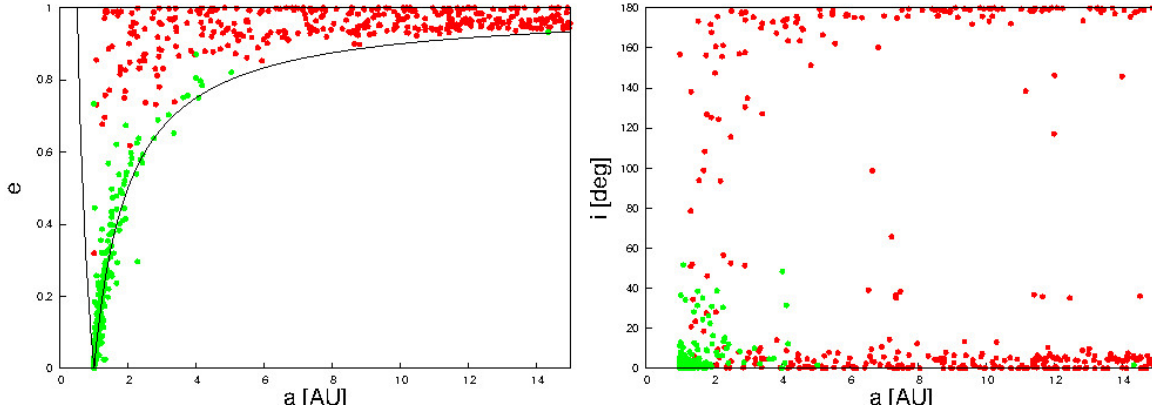


Figure 28: Distribution of orbital elements in the case of *capture* for initial conditions for $i = 30^\circ$, $m = m_J$ after t_{test} . *Left:* Semi-major axis plotted against eccentricity. For planets with initial high inclination it seems unlikely to be captured in orbits with low eccentricity. Although the picture does not look that different from the distribution of orbital elements seen in figure 26. *Right:* Semi-major axis plotted against inclination shows, that more objects are captured in orbits with higher inclination.

Integration times were taken from the interval $[t_{test}; 17.5t_{test}]$ (see section 6.1.3).

Example: For a system with $i = 0.1^\circ$ and $m = m_J$ calculated up to $15t_{test}$ the semi-major axis determined for the captured FFP lies in the range of $0.99AU < a < 319829AU$ where the minimum eccentricity is 0. The bound planet is scattered to orbits with semimajor axis in the range of $0.99AU < a < 663AU$ with a maximum eccentricity of 0.99.

As can be seen in figure 29 after the longer computation time more objects populate orbits with low semi-major axis and low eccentricity (compared to the figures shown before). A wide variety of values for semi-major axis, eccentricity and inclination of the final orbit can be measured. Nevertheless values for semi-major axis and eccentricity do reach relatively low values after the long computation time. This shows, that values for these orbital elements settle down after longer calculation time which can be seen in section 7.2.4 quantitatively.

7.2.4 Capture in orbits with moderate values of semi-major axis and eccentricity

Nevertheless there are not so seldom cases, where the FFP is captured in an orbit with rather moderate values of a and e . Moderate values of a and e in this thesis refers to values in the range of $1r_0 < a < 10r_0$ and $e < 0.8$. If the inclination of the final orbit is considered as well this means the values of the inclination are taken from the range of $i < 15^\circ$.

Motivation behind this is to show, if it is possible, that a captured free-floating planet may stay on an orbit about the star, where it may remain for longer times. A hint for this can be found in the orbital elements of the captured FFP, since orbits with high eccentricity or semi-major axis may decay to a *flyby* after longer integration times.

In order to gain a good overview about the orbital elements of a FFP being captured

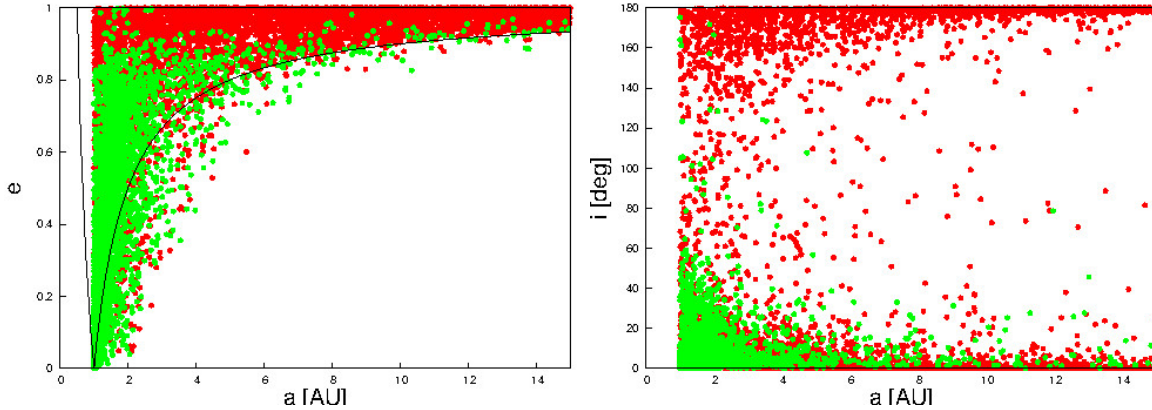


Figure 29: Distribution of orbital elements in the case of *capture* for initial conditions for $i = 0.1^\circ$, $m = m_J$ after $15t_{test}$. *Left hand-side panel:* Semi-major axis plotted against eccentricity. It can be seen, that after this long integration time the BP is scattered to orbits with higher eccentricity and higher semi-major axis, too. *Right hand-side panel:* Semi-major axis plotted against inclination shows, that more objects are captured in orbits with higher inclination and the BP is scattered to orbits with high inclinations.

by a star-planet system the initial value space described above (see section 6.1 - (M, d) with $(0^\circ < M < 360^\circ$ with $\delta M = 0.1^\circ$ and $-7r_0 < d < 7r_0$ with $\delta d = 0.1AU$) is calculated using different values for mass ratio, initial inclination of the FFP and computation time.

In this case only single runs are executed, meaning, that the given values for mass of the FFP, initial inclination and computation time are single values picked from the ranges mentioned in sections 6.1.1, 6.1.2, 6.1.3. With the special value for one of the parameters (mass, inclination, time) each initial condition from the grid of (M, d) is computed.

This means 504000 initial conditions (M, d) being integrated for each set of parameters.

The energy-test is done for each system after the selected computation time. If the final state of the system is classified as *capture*, the orbital parameters of both planets are determined. With this the empirical probabilities for certain ranges of the orbital elements turning up are calculated.

Examples Calculations of trajectories of FFPs with initial inclination of $i = 0.1^\circ$ and $m = m_J$ show that $\sim 0.21\%$ of the captured FFPs end up in orbits with moderate values of semi-major axis and eccentricity.

However, if one demands, that in case of a *capture* both planets stay on an orbit with moderate values of a and e , so that the BP is not scattered to an orbit with high eccentricity or large semi-major axis - which would possibly result in a *exchange* for longer computation time - then the percentage drops to 0.17%.

Comparing these values leads to the assumption, that even if the FFP is captured with low values for the orbital elements the BP may be disturbed from its initial circular orbit due to close encounters and resulting exchange of angular momentum.

Different computation time: For the same initial conditions as above ($i = 0.1^\circ$, $m = m_J$) calculated for longer time-spans of $4t_{test}$ the probability for the orbital ele-

ments of the FFP (measured at the final state of the system) to be *moderate* rises to 0.22%.

Nevertheless in only 0.15% of the calculated systems both planets are on an orbit with the demanded values for a and e at time of the energy-test.

If calculated up to $15t_{test}$ the probabilities rise to 0.36% respectively 0.25% for both planets.

Different initial inclination If the inclination is increased to $i = 5^\circ$ (ceteris paribus) 0.041% of the FFPs are captured in an orbit with moderate values for a and e and in 0.027% cases both planets have moderate values for semi-major axis and eccentricity.

Increasing the initial inclination of the incoming object up to $i = 35^\circ$ lowers the probability for the two objects to stay in orbits with the mentioned moderate values for semi-major axis and eccentricity to 0.016%.

For systems with an initial inclination of the FFP of $i > 40^\circ$ no cases were found were the FFP, not to mention both planets stay in orbits with moderate values for a and e for a calculation time of t_{test} . This fact includes that the probability for a free-floating planet with high initial inclination the *capture* in a long time stable orbit is negligible.

Different mass ratio of the two planets: The probability of a capture of a more massive body of $m = 10m_J$ ($i = 0.1^\circ$ and energy-test done after t_{test}) in an orbit with $a_{FFP} < 10r_0$ and $e_{FFP} < 0.8$ is negligible. More massive intruders tend to occupy orbits with high semi-major axis respectively eccentricity.

Inclination of final orbit In comparison to our solar system, where the highest inclination of an orbit measured is 17.15° in case of the orbit of Pluto the highest final inclination permitted for an orbit in order to be still called orbit with moderate values of orbital elements is set to $i < 15^\circ$.

Comparing the computations from the beginning now yields approximately the same results:

Different initial inclination: 0.1% of systems integrated for $i = 0.1^\circ$, $m = m_J$ up to t_{test} end up so that both planets stay on orbits with the demanded moderate values for semi-major axis, eccentricity and inclination. Increasing the initial inclination of the FFP up to $i = 5^\circ$ (ceteris paribus) decreases the percentage of systems with the demanded values for the final orbital elements to 0.003%. Increasing the initial inclination to $i = 35^\circ$ (ceteris paribus) causes a decrease to 0.002% of systems which end up with the required values for the orbital elements.

Thus, the higher the initial inclination of the intruder, the less likely it is, that in case of a *capture* it occupies an orbit with not only moderate values of a and e but also i .

Different integration time: Increasing the integration time for the systems and executing the energy-test after $15t_{test}$ causes a slight increase in the percentage of systems ending up with moderate values of the final orbital elements of the two bodies to 0.13%.

The same result as observed before is achieved if taking the final inclination of the orbits into account additionally. Longer computation time causes a settlement of

the orbital elements so that after longer timespans more systems fulfil the required restrictions for values of the orbital elements.

Summary: This section shows, that even though the capture of a free-floating object in an orbit with moderate orbital elements is rather unlikely. Nevertheless, it should be pointed out such as the capture in those orbits with moderate values for i , a and e is more likely for lower mass objects with low initial inclination with respect to the entered system.

Additionally as a result of the longer computation time more systems with both planets on orbits with moderate values of semi-major axis, eccentricity and inclination are found.

FFPs being captured on highly eccentric orbits at first (and therefore do not contribute their numbers to the probabilities given for shorter time scales) may settle down to more circular orbits with time.

Results show that the possibility for both, FFP and BP, to be found on an orbit with moderate values a and e increases with time.

This means, the longer a captured body stays in the system, the more its orbital elements seem to level off to values for almost circular orbits, close to the star. Thus it can be said in general, that longer integration periods ensure that the orbital elements of both the FFP and the BP reach lower values. There are two possible explanations for this: Objects which were captured in highly eccentric orbits or orbits with large semi-major axis have left the system before the energy-test was performed and the values for the orbital elements of the final orbits were determined. Therefore they are referred to as *flyby* or *exchange* orbits and are not examined here. The second explanation is valid for less cases. It can be assumed, that the longer the system is calculated, the longer gravitational effects between the two bodies and the captured free-floating planet and the star can act, thus the captured body seems to be drawn to the plane and its values for semi-major axis and eccentricity seem to settle down.

If the initial inclination of the incoming body is increased, the probability to be captured in an orbit with $a < 10r_0$ and $e < 0.8$ decreases. Higher inclination of the FFP leads to capture in more elliptic orbits. These will eventually decay to a flyby or results in a reducing of the probability of close encounters and exchange of angular momentum.

7.2.5 Exchange of orbits

It is possible, that both of the planets exchange positions so that the FFP takes an orbit innermost of the BP.

In $\sim 0.2\%$ of all computations for systems with $i = 0.1^\circ$ and $m = m_J$ this exchange of orbits takes place, where the intruder pushes the bound planet to an orbit outermost of itself.

Inclination: Rising the initial inclination to $i = 35^\circ$ (*ceteris paribus*), causes a decrease in the percentage of systems which end up with the FFP on the innermost orbit to 0.05%.

Mass: Keeping the initial inclination of the FFP fixed to $i = 0.1^\circ$ but rising its mass to $m = 10m_J$ gives a probability for an exchange of positions of $\sim 0.19\%$.

This slightly lower percentage compared to the value for intruders with $m = m_J$ may be explained by the facts derived in section 7.2.1. Captured bodies with higher mass tend to populate orbits with higher values of semi-major axis (see figure 27). Thus a close encounter with the BP and resulting exchange of orbits is unlikely.

Mass, inclination and time: Assuming a mass of $m = 10m_J$ with an inclination of $i = 5^\circ$ results show that in 0.07% of the all systems calculated the FFP takes the inner orbit, if captured around the star.

For the same system with $i = 5^\circ$ and $m = 10m_J$ but now calculated up to $5t_{test}$ results show that in 0.007% of all cases the FFP exchanges its orbit with the bound planet. Thus it can be assumed that if the FFP is captured in an orbit with lower semi-major axis than the bound planet (which may be scattered to an orbit outermost of its initial position) due to the probably high eccentricity of the orbit of the FFP close encounters occur after longer integration time which cause an ejection of one of the two planets or a scattering of the FFP to an again outermost orbit.

Results: As a conclusion it is more likely for a lower mass incoming object with low initial inclination to take the inner orbit in the entered system, as more massive objects tend to stay farther away from the star.

Intruders entering the system with higher inclination have less impact on the orbit of the BP. Due to the initial inclination of the trajectory of the FFP the amount of angular momentum exchanged in case of a close encounter is smaller. This causes fainter impact on the orbit of the BP and therefore minimizes the chance of pushing the BP outwards.

7.3 Prograde and retrograde orbits

Prograde and Retrograde Motion: Prograde motion in case of a solar-like system means motion in the same direction as the rotation of the primary. Retrograde is the direct opposite and refers to a revolution direction of a body opposed to the rotation of the primary.⁵

In general prograde motion refers to motion in the same direction as the other bodies. This definition is used here, because the computation calculates the trajectories for point-masses. In case of a *capture* the orbit of the FFP is referred to as prograde, if the revolution direction is the same as of the bound planet. Retrograde motion describes the revolution direction of the FFP if it is opposed to the one of the BP.⁶

In case of a *capture* of the free-floating planet approximately half of the orbits (the ones with an impact parameter $d > 0$) end up in retrograde orbits. This is caused by the combination of the impact parameter taken from the range of $-7r_0 < d < 7r_0$ and the fixed counterclockwise revolution direction of the BP (see section 5.1).

Cases, where the FFP takes a prograde orbit instead of an expected retrograde orbit or vice versa were observed in general for trajectories with initial conditions where the impact parameter of the FFP is low ($-2r_0 < d < 2r_0$).

However, there are orbits for which the BP changes its original orbital revolution direction from prograde to retrograde or vice versa, but this only happens in 0.003%

⁵https://en.wikipedia.org/wiki/Retrograde_and_prograde_motion

⁶https://en.wikipedia.org/wiki/Retrograde_and_prograde_motion

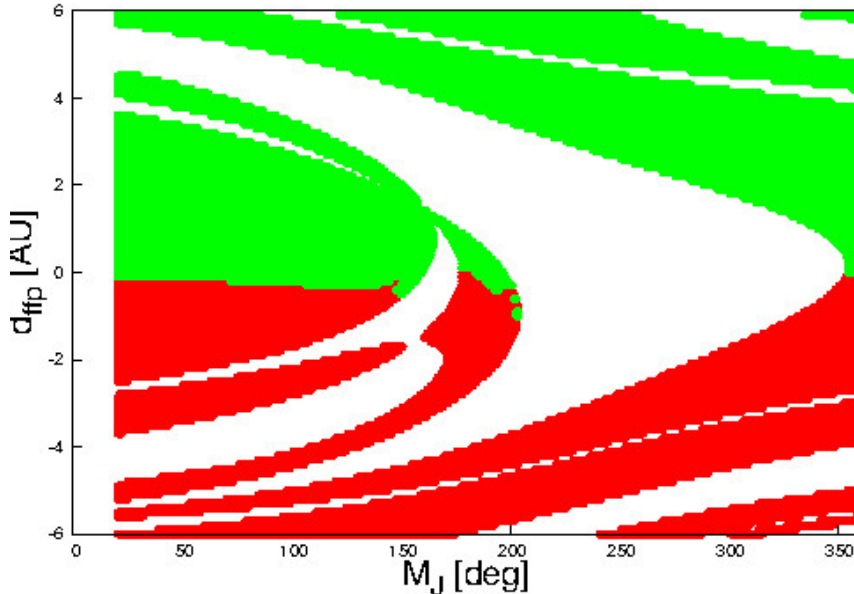


Figure 30: Proportion of *prograde* and *retrograde* orbits for $i = 0.1$ and $m = m_J$ after t_{test} . *Red* dots represent *prograde* and *green* represent *retrograde* orbits. The border between orbits which lead to *retrograde* respectively *prograde* orbits seems to be quite clear at $d \sim 0$ despite some outliers for very low impact parameters.

of all cases (for systems with $i = 0.1^\circ$, $m = m_J$ and the energy-test carried out after t_{test}).

In figure 30 the initial value space for a FFP with $m = m_J$ and an initial inclination of $i = 0.1^\circ$ is shown coded due to the revolution direction at time of the energy-test of the system. *Red* dots represent *prograde* motion of the captured object and *green* *retrograde* revolution direction.

The border between the two basins looks quite smooth at $d = 0$ despite from some small spikes between values of the mean anomaly of the bound planet in the range of $130^\circ < M < 210^\circ$. Retrograde orbits (*green*) occurring marginally under the borderline to the other basin of $d = 0$ appear in general for systems with $M < 210^\circ$ and for $-1 < d < 0$.

For changing the revolution direction of a planet the exchange of angular momentum is necessary. The closer the two bodies get, the more powerful this process is. Thus, it is more likely for FFPs with a small impact parameter d , where the two planets can come very close to each other, to take the opposite of its expected revolution direction.

Nevertheless this process depends on the relative phase of the two bodies, too. This is affected by the mean anomaly M of the initial orbit of the BP. As can be seen in figure 30, where for $M < 210^\circ$ retrograde orbits (*green*) appear for small negative values of the impact parameter d . Some isolated *green* points indicating a retrograde orbit of the captured free-floating planet in the basin of prograde motion are visible at $M \sim 205^\circ$ for an impact parameter as small as $d = -1$.

For initial conditions $i = 0.1^\circ$ and $m = m_J$ after t_{test} 47.39% of the FFPs end up in prograde orbits. Thus, 52.61% of the incoming objects were captured in retrograde motion.

7.3.1 Bound planet driven to retrograde orbit

As mentioned already, the probability for a case, where the BP is driven to an orbit with different revolution direction, is very low, nevertheless those cases are possible.

This can be observed from figure 27 (see section 7.2.2), where one can see that there are some cases, where the BP is forced to change its original revolution direction (so that $i_{BP} > 90^\circ$). This cases occur for cases with more massive incoming free-floating planets and can be explained by the calculated energy between the bodies in pairs, which shows that for a massive FFP, the energy of the FFP-BP pair becomes non negligible. So the amount of angular momentum exchanged is higher for more massive incoming objects.

The same explanation as mentioned above can be used here to explain this phenomenon: Probably a close encounter or the crossing of a resonance and thus strong interactions between the two acting planets may be the case why the BP changes its initial revolution direction.

7.4 Different initial velocity of incoming body

For all other computations, as mentioned in the beginning, the trajectories were calculated with a parabolic velocity of the FFP (see section 5.1, equation 5.1).

Motivation: In order to investigate the influence of the initial velocity of the incoming body on the scattering process, two scenarios with an initial velocity higher and lower than the parabolic one were computed. It was expected to gain knowledge about cases, where the incoming free-floating planet in the possible surrounding of a cluster enters a bound system with different velocity than the particular parabolic velocity. Since it might well be possible that due to gravitational interaction with other stars or planetary systems the free-floating object has gained or lost speed before it reaches the regarded system.

The system of three bodies was calculated for all sets of initial conditions of (d, M) in the already known ranges of $0^\circ < M < 360^\circ$ with $\delta M = 0.1$ and $-7r_0 < d < 7r_0$ with $\delta d = 0.1AU$. The initial inclination of the incoming body was set and fixed to the value of $i = 5^\circ$ in order to fulfil the requirement of three dimensional computations but don't include effects resulting from high initial inclination.

Computing the trajectories for an initial velocity of the FFP 10% higher than the parabolic one (a case for which the total Energy of the system still stays negative), the probability of *capture* decreases strongly. This corresponds to the expectations. A higher velocity makes it easier for the object to escape the gravitational influence of the bound system. Thus the case of *flyby* becomes more likely.

Only 6.45% of all fast free-floating Jupiter-sized planets with initial inclination of $i = 5^\circ$ are found to stay in the state of *capture* by executing the energy-test at t_{test} . This value is remarkably low compared to 56.64% of *captures* when using an initial parabolic velocity of the intruder.

For a velocity 10% lower than the parabolic one the probability of *capture* increases to 92.25% if calculating the trajectories for *ceteris paribus*.

Different mass of intruder with lower velocity: If one considers the mass of the incoming planet as low as $m = 10^{-7}m_J$ which refers to approximately the mass of

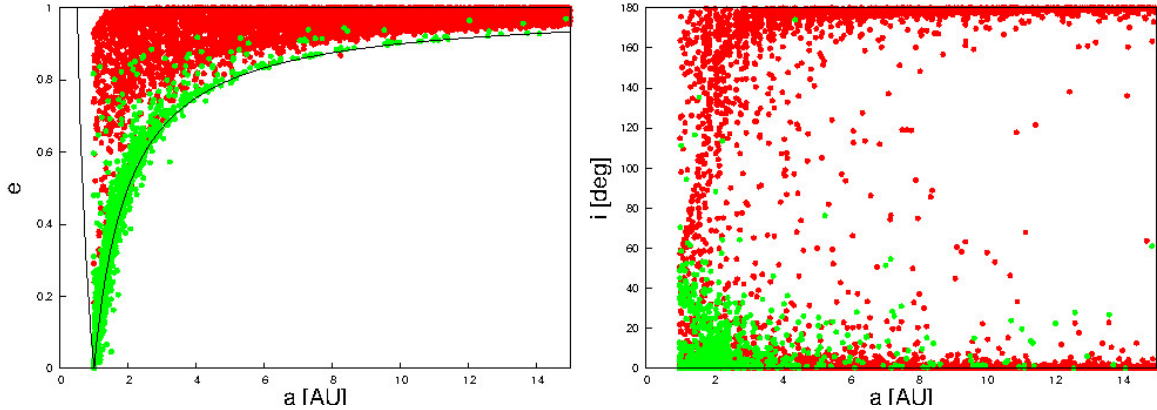


Figure 31: Distribution of orbital elements in the case of *capture* for initial conditions for $i = 0.1^\circ$, $m = m_J$ after t_{test} but for a initial velocity being $0.9v_0$. *Left hand-side panel:* Semi-major axis plotted against eccentricity. Where *red* dots represent the orbital elements of the FFP at time of the final state of the system and *green* dots the orbital parameters of the bound planet. Constant apocenter- and pericenter-curves are shown as black lines. *Right hand-side panel:* Semi-major axis plotted against inclination for the FFP and the BP at time of the final state of the system.

Ganymede and computes the trajectories for the initial velocity of 10% lower than the parabolic one, the picture only changes slightly. 92.59% of the free-floating objects end up on a *captured* orbit around the star. However the capture of the incoming object as a moon of the bound Jupiter did not occur in the computations.

Different initial inclination and computation time: Approximately the same values for the probabilities of *capture* as shown above were observed for systems calculated with higher values of the initial inclination of the incoming body up to $i = 45^\circ$ and for calculations on longer time scales. For objects with a initial velocity of 10% higher than the parabolic one probabilities for a *capture* were always $< 10\%$ and for systems with initial velocity 10% lower than the parabolic one the corresponding values derived were always $> 90\%$.

The orbital elements of the final orbits of the FFP (*red*) and the bound planet (*green*) are plotted in figure 31. Compared to the figures shown in section 7.2.4 one can see, that not so few FFPs populate the regions with low semi-major axis coupled with relatively low eccentricity (see figure 31 - *left hand-side* panel). On the other hand a lot of bound planets (*green*) are scattered to orbits with high eccentricities and even to orbits with semi-major axes up to more than $10AU$.

This can also be reproduced by examining the percentages of systems where the planets stay on orbits with moderate values of semi-major axis and eccentricity (see section 7.2.4). In only 0.05% of all cases calculated for $i = 0.1^\circ$, $m = m_J$ and an initial velocity of the incoming object being $0.9v_0$ both planets stay on orbits with moderate values of semi-major axis and eccentricity which on the other hand means that in most cases at least one of the planets inherits an orbit which is highly eccentric or has a large semi-major axis and is therefore probably not long-time stable.

If one requires the values for the inclination of the final orbits being $< 15^\circ$ the percentage of systems where both planets stay on orbits with additional moderate values for a and e drops to 0.02%.

This shows, that despite the lower initial velocity the capture of a free-floating planet on an orbit which may be stable for longer times does not become more likely than for FFPs with initial parabolic velocity. On the contrary the percentage of systems ending up with the required values for semi-major axis and eccentricity drops.

8 Summary and Conclusions

Observations and extensions of the galactic mass-function show that free-floating objects with $M < 13M_J$ are more common, than was assumed. (Sumi et al., 2011; Zapatero Osorio et al., 2000) Thus, it is interesting to investigate, what happens if a free-floating planet enters a gravitationally bound planetary system. Therefore in the presented Master's thesis the interaction of a free-floating planetary object with an existing simplified planetary system consisting of a star and a Jupiter-sized planet was studied. Incoming from "infinity" is a free-floating planet interacting with the system.

The impact parameter d , the initial inclination i of the incoming object and the phase of the bound Jupiter were varied in order to investigate the influence of those parameters on the scattering process. d was varied in the range of $-7r_0 \leq d \leq 7r_0$ and the value for i was picked between 0° and 90° . Additionally the mass of the incoming object was changed in the range of $10^{-7}m_J < m < 10m_J$.

Three possible outcomes occur as there are *flyby*, *exchange* and *capture*.

The first thing to mention is, that the scattering process is chaotic, meaning, that the prediction of the final state with the knowledge of only the initial values of the planet's trajectory is not possible with a hundred percent certainty for all initial conditions and therefore a statistical approach is the best way to deal with the data.

What can be observed is that the probability of *capture* of the FFP is varying with its mass. In general it can be said, that the probability for a *capture* of the intruding object increases with mass. And is derived in the range of 55.85% to 56.12%. Interesting is the minimum of the probability of a *capture* for incoming objects with a mass of $m = 3m_J$, which needs further investigation. The probability of *exchange* of the two planets, meaning that the incoming planet takes a bound orbit and the initially bound planet is ejected from its system, is increasing with mass of the intruder. For an incoming object with $m < 0.5m_J$ *exchange* is not possible. The percentage of trajectories ending up as *flyby* is increasing with mass of the incoming object.

Calculating the probability of *capture* depending on the initial inclination of the incoming free-floating object shows an exponential decrease of the values for the probability which does not go to zero for values as high as $i = 88^\circ$. The percentage of trajectories ending up in a *captured* orbit varies between 58.98% and 29.85%. Thus the initial inclination of the incoming free-floating object has the highest measured influence on the final state besides mass and time. The probability of an *exchange* is $\sim 0^\circ$ for values of the initial inclination of $i > 5^\circ$. However, if calculating the trajectories for incoming objects with initial inclination $i > 5^\circ$ for longer time scales ($t > t_{test}$) shows, that *exchange* orbits do occur for this values of initial inclination. This may be because objects which are captured on highly eccentric orbits undergo close encounters with the bound Jupiter after some longer calculation times which lead to an ejection of the BP and therefore only contribute to the percentage of *exchange* if longer time scales are taken into account.

Time as parameter does not have a strong influence on the probability of the three outcomes. The percentage of trajectories ending in the final state of *capture* varies between 56.13% and 55.46%.

From the previous results it is stated, that the *capture* of a free-floating planet on an orbit in an existing bound system is possible. Furthermore it could be shown that FFPs can be captured in orbits with moderate values of a and e , meaning values of $a < 10AU$ and $e < 0.8$ and accordingly $i < 15^\circ$. In most of these cases, the BP is

excited to an orbit with higher values of e and inclination, i . However, there are a few cases ($\sim 0.17\%$ for systems with $i = 0.1^\circ$ and $m = m_J$), where both planets stay on orbits with low values of a and e around the star. This percentage rises with calculation time. For example for $15t_{test}$ the probability for both planets to stay on orbits with $a < 10AU$ and $e < 0.8$ rises to 0.25% .

This result is interesting concerning the perspective on exoplanetary systems because one could conclude, that maybe some exoplanets are in fact captured free-floating planets (especially exoplanetary systems with planets on highly inclined or highly eccentric orbits. As the *capture* in orbits with high values for eccentricity and semi-major axis is more probable).

Important to mention is the fact, that *capture* in retrograde orbits is possible. This happens for approximately half of the cases depending on the impact parameter d of the incoming free-floating planet.

Additionally the investigation of the influence of the initial velocity of the incoming planetary object confirms the expectations. A velocity 10% lower as the normally used parabolic velocity leads to a strong increase of the probability of *capture* while a velocity 10% higher leads to a strong decrease of the probability of orbits which end up in *capture*.

To sum it up the following conclusions can be made: Higher mass of the incoming free-floating planet causes an increase of the probability of being *captured*. An increase of the initial inclination of the intruder causes a decrease of the probability of *capture*. Higher integration time shows less free-floating planets ending up in the state of *capture* after the energy-test. Possible explanation for this may be close encounters or the crossing of resonances after several revolution periods which cause ejection of one of the two planets. *Capture* in both prograde and retrograde orbits is possible.

Concerning the orbital elements in case of a capture it is shown that free-floating planets with higher mass tend to be captured in orbits with higher semi-major axis and relatively low eccentricity and inclination. As a consequence of higher initial inclination of the incoming object the probability of being captured in an orbit with moderate values of semi-major axis and eccentricity decreases. (Moderate values refer to values for the semi-major axis $a < 10AU$, eccentricity $e < 0.8$ and inclination of the final orbit $i < 15^\circ$.) Longer calculation time shows, that the orbital elements settle down over time. Thus after longer integration time the captured objects show lower values for eccentricity and inclination.

An initial velocity different from the parabolic one causes the expected results: lower initial velocity leads to an increased number of objects ending up in *capture* while higher initial velocity causes the opposite. Nevertheless only 0.05% of the systems with an incoming object with $v = 0.9v_0$ (initial velocity being 90% of the parabolic one) end up with moderate values for the orbital elements of the planets.

Outlook: It would be interesting to study the long term stability of systems which end up in the state of *capture* with moderate values of semi-major axis and eccentricity. Maybe applying the Lyapunov would yield interesting results.

The influence of an incoming planetary object on a solar-like system with more bodies would be interesting to compute but was unfortunately too time extensive to be implemented in this thesis.

Another aspect of dealing with the capture of free-floating planets might be to model existing exoplanetary systems which have known planetary components orbiting

on retrograde orbits or on orbits with high values for semi-major axis, eccentricity or inclination in order to find out, if it is possible, that one of the planetary bodies is in fact a captured free-floating planet.

Orbital parameters can as well be taken in order to show if a FFP may be captured in an orbit not only with moderate values for its orbital elements but in the habitable zone of its new host star. And if it is possible that it can stay there on a long-term stable habitable orbit. Nevertheless this would have gone beyond the volume of this thesis.

9 Acknowledgements

At this point I would like to thank all those people who supported me in the development of this Master's thesis.

It is with immense gratitude, that I acknowledge the support and help of Prof. Dr. Rudolf Dvorak, who always encouraged me in proceeding with my thesis and had plenty of patience in waiting for results. I am thankful, that he had time for me whenever I needed professional advice.

Special thanks to Daniel Steiner, who always had time to offer me advice and help with Linux- and Latex-matters and to Karl Schwaiger for his critical view and productive council concerning the writing of my thesis.

Last but not least I want to thank my parents for believing in me and for their financial support providing me the opportunity to study.

References

- F. C. Adams, E. M. Proszkow, M. Fatuzzo, and P. C. Myers. Early Evolution of Stellar Groups and Clusters: Environmental Effects on Forming Planetary Systems. *ApJ*, 641:504–525, April 2006. doi: 10.1086/500393.
- V. Badescu. Free-floating planets as potential seats for aqueous and non-aqueous life. *Icarus*, 216:485–491, December 2011. doi: 10.1016/j.icarus.2011.09.013.
- D. P. Bennett, V. Batista, I. A. Bond, C. S. Bennett, D. Suzuki, J.-P. Beaulieu, A. Udalski, J. Donatowicz, V. Bozza, F. Abe, C. S. Botzler, M. Freeman, D. Fukunaga, A. Fukui, Y. Itow, N. Koshimoto, C. H. Ling, K. Masuda, Y. Matsubara, Y. Muraki, S. Namba, K. Ohnishi, N. J. Rattenbury, T. Saito, D. J. Sullivan, T. Sumi, W. L. Sweatman, P. J. Tristram, N. Tsurumi, K. Wada, P. C. M. Yock, MOA Collaboration, M. D. Albrow, E. Bachelet, S. Brilliant, J. A. R. Caldwell, A. Cassan, A. A. Cole, E. Corrales, C. Coutures, S. Dieters, D. Dominis Prester, P. Fouqué, J. Greenhill, K. Horne, J.-R. Koo, D. Kubas, J.-B. Marquette, R. Martin, J. W. Menzies, K. C. Sahu, J. Wambsganss, A. Williams, M. Zub, PLANET Collaboration, J. Y. Choi, D. L. DePoy, S. Dong, B. S. Gaudi, A. Gould, C. Han, C. B. Henderson, D. McGregor, C.-U. Lee, R. W. Pogge, I.-G. Shin, J. C. Yee, μ FUN Collaboration, M. K. Szymański, J. Skowron, R. Poleski, S. Kozłowski, Ł. Wyrzykowski, M. Kubiak, P. Pietrukowicz, G. Pietrzyński, I. Soszyński, K. Ulaczyk, OGLE Collaboration, Y. Tsapras, R. A. Street, M. Dominik, D. M. Bramich, P. Browne, M. Hundertmark, N. Kains, C. Snodgrass, I. A. Steele, The RoboNet Collaboration, I. Dekany, O. A. Gonzalez, D. Heyrovský, R. Kandori, E. Kerins, P. W. Lucas, D. Minniti, T. Nagayama, M. Rejkuba, A. C. Robin, and R. Saito. MOA-2011-BLG-262Lb: A Sub-Earth-Mass Moon Orbiting a Gas Giant Primary or a High Velocity Planetary System in the Galactic Bulge. *ApJ*, 785:155, April 2014. doi: 10.1088/0004-637X/785/2/155.
- O. Benomar, K. Masuda, H. Shibahashi, and Y. Suto. Determination of Three-dimensional Spin-orbit Angle with Joint Analysis of Asteroseismology, Transit Lightcurve, and the Rossiter-McLaughlin Effect: Cases of HAT-P-7 and Kepler-25. *ArXiv e-prints*, July 2014.
- G. Bihain, R. Rebolo, M. R. Zapatero Osorio, V. J. S. Béjar, I. Villó-Pérez, A. Díaz-Sánchez, A. Pérez-Garrido, J. A. Caballero, C. A. L. Bailer-Jones, D. Barrado y Navascués, J. Eislöffel, T. Forveille, B. Goldman, T. Henning, E. L. Martín, and R. Mundt. Candidate free-floating super-Jupiters in the young σ Orionis open cluster. *A&A*, 506:1169–1182, November 2009. doi: 10.1051/0004-6361/200912210.
- S. Bleher, C. Grebogi, and E. Ott. Bifurcation to chaotic scattering. *Physica D Nonlinear Phenomena*, 46:87–121, October 1990. doi: 10.1016/0167-2789(90)90114-5.
- P. T. Boyd and S. L. W. McMillan. Chaotic scattering in the gravitational three-body problem. *Chaos*, 3:507–523, October 1993. doi: 10.1063/1.165956.
- D. Branch. On the Multiplicity of Solar-Type Stars. *ApJ*, 210:392–394, December 1976. doi: 10.1086/154841.

- J. I. Canty, P. W. Lucas, P. F. Roche, and D. J. Pinfield. Towards precise ages and masses of Free Floating Planetary Mass Brown Dwarfs. *MNRAS*, 435:2650–2664, November 2013. doi: 10.1093/mnras/stt1477.
- P. Delorme, J. Gagné, L. Malo, C. Reylé, E. Artigau, L. Albert, T. Forveille, X. Delfosse, F. Allard, and D. Homeier. CFBDSIR2149-0403: a 4-7 Jupiter-mass free-floating planet in the young moving group AB Doradus? *A&A*, 548:A26, December 2012a. doi: 10.1051/0004-6361/201219984.
- P. Delorme, J. Gagné, L. Malo, C. Reylé, E. Artigau, L. Albert, T. Forveille, X. Delfosse, F. Allard, and D. Homeier. CFBDSIR2149-0403: a 4-7 Jupiter-mass free-floating planet in the young moving group AB Doradus? *A&A*, 548:A26, December 2012b. doi: 10.1051/0004-6361/201219984.
- J. R. Donnison. The Hill stability of a binary or planetary system during encounters with a third inclined body. *MNRAS*, 369:1267–1280, July 2006. doi: 10.1111/j.1365-2966.2006.10372.x.
- M. Esposito, E. Covino, L. Mancini, A. Harutyunyan, J. Southworth, K. Biazzo, D. Gandolfi, A. F. Lanza, M. Barbieri, A. S. Bonomo, F. Borsa, R. Claudi, R. Cosentino, S. Desidera, R. Gratton, I. Pagano, A. Sozzetti, C. Boccato, A. Maggio, G. Micela, E. Molinari, V. Nascimbeni, G. Piotto, E. Poretti, and R. Smareglia. The GAPS Programme with HARPS-N at TNG. III: The retrograde orbit of HAT-P-18b. *A&A*, 564:L13, April 2014. doi: 10.1051/0004-6361/201423735.
- G. F. Gahm, C. M. Persson, M. M. Mäkelä, and L. K. Haikala. Mass and motion of globulets in the Rosette Nebula. *A&A*, 555:A57, July 2013. doi: 10.1051/0004-6361/201321547.
- A. Gould, J. Pepper, and D. L. DePoy. Sensitivity of Transit Searches to Habitable-Zone Planets. *ApJ*, 594:533–537, September 2003. doi: 10.1086/376852.
- C. Han. Secure Identification of Free-floating Planets. *ApJ*, 644:1232–1236, June 2006. doi: 10.1086/503890.
- C. Han, S.-J. Chung, D. Kim, B.-G. Park, Y.-H. Ryu, S. Kang, and D. W. Lee. Gravitational Microlensing: A Tool for Detecting and Characterizing Free-Floating Planets. *ApJ*, 604:372–378, March 2004. doi: 10.1086/381429.
- A. Hanslmeier and R. Dvorak. Numerical Integration with Lie Series. *A&A*, 132:203, March 1984.
- C. B. Henderson, B. S. Gaudi, C. Han, J. Skowron, M. T. Penny, D. Nataf, and A. P. Gould. Optimal Survey Strategies and Predicted Planet Yields for the Korean Microlensing Telescope Network. *ArXiv e-prints*, June 2014.
- G. W. Hill. On Dr. Weiler’s Secular Acceleration of the Moon’s mean Motion. *Astronomische Nachrichten*, 91:251, January 1878. doi: 10.1002/asna.18780911605.
- J. R. Hurley and M. M. Shara. Free-floating Planets in Stellar Clusters: Not So Surprising. *ApJ*, 565:1251–1256, February 2002. doi: 10.1086/337921.

- V. Joergens, M. Bonnefoy, Y. Liu, A. Bayo, and S. Wolf. The Coolest ‘Stars’ are Free-Floating Planets. In G. T. van Belle and H. C. Harris, editors, *Cambridge Workshop on Cool Stars, Stellar Systems, and the Sun*, volume 18 of *Cambridge Workshop on Cool Stars, Stellar Systems, and the Sun*, pages 1019–1026, January 2015.
- P. Kroupa and J. Bouvier. On the origin of brown dwarfs and free-floating planetary-mass objects. *MNRAS*, 346:369–380, December 2003. doi: 10.1046/j.1365-2966.2003.07224.x.
- M. C. Liu, E. A. Magnier, N. R. Deacon, K. N. Allers, T. J. Dupuy, M. C. Kotson, K. M. Aller, W. S. Burgett, K. C. Chambers, P. W. Draper, K. W. Hodapp, R. Jedicke, N. Kaiser, R.-P. Kudritzki, N. Metcalfe, J. S. Morgan, P. A. Price, J. L. Tonry, and R. J. Wainscoat. The Extremely Red, Young L Dwarf PSO J318.5338-22.8603: A Free-floating Planetary-mass Analog to Directly Imaged Young Gas-giant Planets. *ApJ*, 777:L20, November 2013a. doi: 10.1088/2041-8205/777/2/L20.
- M. C. Liu, E. A. Magnier, N. R. Deacon, K. N. Allers, T. J. Dupuy, M. C. Kotson, K. M. Aller, W. S. Burgett, K. C. Chambers, P. W. Draper, K. W. Hodapp, R. Jedicke, N. Kaiser, R.-P. Kudritzki, N. Metcalfe, J. S. Morgan, P. A. Price, J. L. Tonry, and R. J. Wainscoat. The Extremely Red, Young L Dwarf PSO J318.5338-22.8603: A Free-floating Planetary-mass Analog to Directly Imaged Young Gas-giant Planets. *ApJ*, 777:L20, November 2013b. doi: 10.1088/2041-8205/777/2/L20.
- D. Malmberg, F. de Angeli, M. B. Davies, R. P. Church, D. Mackey, and M. I. Wilkinson. Close encounters in young stellar clusters: implications for planetary systems in the solar neighbourhood. *MNRAS*, 378:1207–1216, July 2007. doi: 10.1111/j.1365-2966.2007.11885.x.
- C. Marchal and G. Bozis. Hill Stability and Distance Curves for the General Three-Body Problem. *Celestial Mechanics*, 26:311–333, March 1982. doi: 10.1007/BF01230725.
- M. Mayor and D. Queloz. A Jupiter-mass companion to a solar-type star. *Nature*, 378:355–359, November 1995. doi: 10.1038/378355a0.
- K. Mužić, A. Scholz, V. C. Geers, R. Jayawardhana, M. Tamura, P. Dawson, and T. P. Ray. The SONYC survey: Towards a complete census of brown dwarfs in star forming regions. *Mem. Soc. Astron. Italiana*, 84:931, 2013.
- H. Poincare. *New methods of celestial mechanics*. 1993.
- S. P. Quanz, B. Goldman, T. Henning, W. Brandner, A. Burrows, and L. W. Hofstetter. Search for Very Low-Mass Brown Dwarfs and Free-Floating Planetary-Mass Objects in Taurus. *ApJ*, 708:770–784, January 2010. doi: 10.1088/0004-637X/708/1/770.
- L. E. Strigari, M. Barnabè, P. J. Marshall, and R. D. Blandford. Nomads of the Galaxy. *MNRAS*, 423:1856–1865, June 2012. doi: 10.1111/j.1365-2966.2012.21009.x.
- T. Sumi. Current and Future of Microlensing Exoplanet Search. In N. Haghhighipour, editor, *IAU Symposium*, volume 293 of *IAU Symposium*, pages 10–19, April 2014. doi: 10.1017/S1743921313012453.

- T. Sumi, K. Kamiya, D. P. Bennett, I. A. Bond, F. Abe, C. S. Botzler, A. Fukui, K. Furusawa, J. B. Hearnshaw, Y. Itow, P. M. Kilmartin, A. Korpela, W. Lin, C. H. Ling, K. Masuda, Y. Matsubara, N. Miyake, M. Motomura, Y. Muraki, M. Nagaya, S. Nakamura, K. Ohnishi, T. Okumura, Y. C. Perrott, N. Rattenbury, T. Saito, T. Sako, D. J. Sullivan, W. L. Sweatman, P. J. Tristram, A. Udalski, M. K. Szymański, M. Kubiak, G. Pietrzyński, R. Poleski, I. Soszyński, Ł. Wyrzykowski, K. Ulaczyk, and Microlensing Observations in Astrophysics (MOA) Collaboration. Unbound or distant planetary mass population detected by gravitational microlensing. *Nature*, 473:349–352, May 2011. doi: 10.1038/nature10092.
- H. Varvoglis, V. Sgardeli, and K. Tsiganis. Interaction of free-floating planets with a star-planet pair. *Celestial Mechanics and Dynamical Astronomy*, 113:"387–402", August 2012. doi: "10.1007/s10569-012-9429-8".
- A. Wolszczan and D. A. Frail. A planetary system around the millisecond pulsar PSR1257 + 12. *Nature*, 355:145–147, January 1992. doi: 10.1038/355145a0.
- M. M. Woolfson. The capture theory and the inclinations of exoplanet orbits. *MNRAS*, 436:1492–1496, December 2013. doi: 10.1093/mnras/stt1668.
- J. T. Wright and B. S. Gaudi. *Exoplanet Detection Methods*, page 489. 2013. doi: 10.1007/978-94-007-5606-9_10.
- M. R. Zapatero Osorio, V. J. S. Béjar, R. Rebolo, E. L. Martín, and G. Basri. An L-Type Substellar Object in Orion: Reaching the Mass Boundary between Brown Dwarfs and Giant Planets. *ApJ*, 524:L115–L118, October 1999. doi: 10.1086/312317.
- M. R. Zapatero Osorio, V. J. S. Béjar, E. L. Martín, R. Rebolo, D. Barrado y Navascués, C. A. L. Bailer-Jones, and R. Mundt. Discovery of Young, Isolated Planetary Mass Objects in the σ Orionis Star Cluster. *Science*, 290:103–107, October 2000. doi: 10.1126/science.290.5489.103.
- M. R. Zapatero Osorio, V. J. S. Béjar, E. L. Martín, R. Rebolo, D. Barrado Y Navascués, C. A. L. Bailer-Jones, and R. Mundt. Evidence for Free-floating Planetary-mass Objects in the σ Orionis Star Cluster (CD-ROM Directory: contribs/osorio). In R. J. Garcia Lopez, R. Rebolo, and M. R. Zapaterio Osorio, editors, *11th Cambridge Workshop on Cool Stars, Stellar Systems and the Sun*, volume 223 of *Astronomical Society of the Pacific Conference Series*, page 70, 2001.
- M. R. Zapatero Osorio, V. J. S. Béjar, and K. Peña Ramírez. Optical and near-infrared spectroscopy of free-floating planets in the sigma Orionis cluster. *Mem. Soc. Astron. Italiana*, 84:926, 2013.
- M. R. Zapatero Osorio, M. C. Gálvez Ortiz, G. Bihain, C. A. L. Bailer-Jones, R. Rebolo, T. Henning, S. Boudreault, V. J. S. Béjar, B. Goldman, R. Mundt, and J. A. Caballero. Search for free-floating planetary-mass objects in the Pleiades. *ArXiv e-prints*, July 2014.
- H. Zinnecker. A Free-Floating Planet Population in the Galaxy? In J. W. Menzies and P. D. Sackett, editors, *Microlensing 2000: A New Era of Microlensing Astrophysics*, volume 239 of *Astronomical Society of the Pacific Conference Series*, page 223, 2001.

List of Figures

1	Experimental setup - 3D	14
2	Example for a <i>capture</i> and <i>exchange</i> orbit.	19
3	Example for a <i>flyby</i>	19
4	Example for a <i>capture</i> which develops to an <i>exchange</i>	20
5	Example for a <i>capture</i> which develops to a <i>flyby</i>	20
6	Evolution of orbital elements for $t = 6.5t_{test}$	22
7	Evolution of orbital elements for $t = 31.5t_{test}$	23
8	Evolution of orbital elements for $t = 4t_{test}$	24
9	Evolution of orbital elements for $t = 31.5t_{test}$	25
10	Initial value space for $m = 3m_J$, $i = 0.1^\circ$ after $t = 2t_{test}$	27
11	Magnifications of initial value space, fractal borders visible.	27
12	<i>Epsilon uncertainty</i>	29
13	Initial value space for $m = 0.0001m_J$ and $m = 0.5m_J$	31
14	Initial value space for $m = 1m_J$ and $m = 5m_J$	31
15	Initial value space for $m = 10m_J$	32
16	Initial value space for $i = 5^\circ$ and $i = 18^\circ$	33
17	Initial value space for $i = 35^\circ$	34
18	Initial value space for $t = test$ and $t = 17.5t_{test}$	35
19	Probabilities for <i>capture</i> and <i>exchange</i> as function of the mass of the FFP.	37
20	Probabilities for <i>capture</i> and <i>exchange</i> as function of initial inclination i of the FFP.	39
21	Probabilities for <i>capture</i> and <i>flyby</i> as function of calculation time.	41
22	Part of <i>prograde</i> and <i>retrograde</i> orbits for $i = 10^\circ$ and $m = m_J$ after t_{test}	43
23	Part of <i>prograde</i> and <i>retrograde</i> orbits for $i = 40^\circ$ and $m = m_J$ after t_{test}	43
24	Part of <i>prograde</i> and <i>retrograde</i> orbits for $i = 0.1$ and $m = 10m_J$ after t_{test}	44
25	Part of <i>prograde</i> and <i>retrograde</i> orbits for $i = 0.1$ and $m = m_J$ after $t = 16t_{test}$	45
26	Orbital elements for FFPs with $i = 0.1^\circ$, $m = m_J$ after t_{test}	49
27	Orbital elements for FFPs with $i = 0.1^\circ$, $m = 5m_J$ after t_{test}	50
28	Orbital elements for FFPs with $i = 30^\circ$, $m = m_J$ after t_{test}	51
29	Orbital elements for FFPs with $i = 0.1^\circ$, $m = m_J$ after $15t_{test}$	52
30	Part of <i>prograde</i> and <i>retrograde</i> orbits for $i = 0.1$ and $m = m_J$ after t_{test}	56

Curriculum Vitae:

Birgit Loibnegger

Education:

2015	Master of Astronomy
2010	Bachelor of Astronomy Bachelorthesis on 'Astroseismologische Weltraummissionen'
2006-2015	University Studies of Astronomy, University of Vienna, Institute for Astrophysics, Türkenschanzstraße 17, 1180 Wien
2007-2010	University Studies of Physics and German Philology, University of Vienna
1998-2006	High School, Realgymnasium Tulln, Donaulände 72, 3430 Tulln

Employment:

2015 May-Sept.	Contract for work within the scope of the NFN project 'Pathways to Habitability' Short Title: 'Transport of Water in Early Planetary Systems' Description: Detailed investigations of the formation of terrestrial planets depending on their water content using modified n-body integrators on the collision outcome
----------------	--

List of Publications:

Loibnegger, B.

On the Capture of Free-Floating Planets, Master's Thesis, submitted

Dvorak, R.; Maindl, T.I.; *Loibnegger, B.*

On the probability of the collision of a Mars-sized planet with the Earth to form the Moon, MNRAS, submitted

Loibnegger, B.; Varvoglis, H.; Dvorak, R.

On the diversity of free-floating planets, CMDA, in preparation